Importance of *Angomonas deanei* KAP4 for kDNA arrangement, cell division and maintenance of the host-bacterium relationship

Camila Silva Gonçalves[1,2‖], Carolina Moura Costa Catta-Preta[3‖], Bruno Repolês[4], Jeremy C. Mottram[3], Wanderley de Souza[1,2], Carlos Renato Machado[4*], Maria Cristina M. Motta[1,2*]

[1]Laboratório de Ultraestrutura Celular Hertha Meyer, Instituto de Biofísica Carlos Chagas Filho, Universidade Federal do Rio de Janeiro, 21491-590, Rio de Janeiro, RJ, Brazil.

[2]Instituto Nacional de Ciência e Tecnologia em Biologia Estrutural e Bioimagem – RJ, Brazil.

[3]York Biomedical Research Institute, Department of Biology, University of York, Wentworth Way, Heslington, York, YO10 5DD, UK.

[4]Laboratório de Genética Bioquímica, Departamento de Bioquímica e Imunologia, Instituto de Ciências Biológicas, Universidade Federal de Minas Gerais, Belo Horizonte, Brazil.

‖Both authors contributed equally to this scientific article

*Corresponding authors: Maria Cristina M. Motta, motta@biof.ufrj.br, Laboratório de Ultraestrutura Celular Hertha Meyer, IBCCF, CCS, UFRJ, Cidade Universitária, Rio de Janeiro, CEP 21941-590, Brazil. Carlos Renato Machado, crmachad@icb.ufmg.br, Laboratório de Genética Bioquímica, Departamento de Bioquímica e Imunologia, Instituto de Ciências Biológicas, Universidade Federal de Minas Gerais, Belo Horizonte, Brazil.

Abstract

Angomonas deanei coevolves in a mutualistic relationship with a symbiotic bacterium that divides in synchronicity with other host cell structures. Trypanosomatid mitochondrial DNA is contained in the kinetoplast and is composed of thousands of interlocked DNA circles (kDNA). The arrangement of kDNA is related the presence of histone-like proteins, known as KAPs (kinetoplast-associated proteins), that neutralize the negatively charged kDNA, thereby affecting the activity of mitochondrial enzymes involved in replication, transcription and repair. In this study, CRISPR-Cas9 was used to delete both alleles of the *A. deanei KAP4* gene. Gene-deficient mutants exhibited high compaction of the kDNA network and displayed atypical phenotypes, such as the appearance of a filamentous symbionts, cells containing two nuclei and one kinetoplast, and division blocks. Treatment with cisplatin and UV showed that Δ*kap4* null mutants were not more sensitive to DNA damage and repair than wild-type cells. Notably, lesions caused by these genotoxic agents in the mitochondrial DNA could be repaired, suggesting that the kDNA in the kinetoplast of trypanosomatids has unique repair mechanisms. Taken together, our data indicate that although KAP4 is not an essential protein, it plays important roles in kDNA arrangement and replication, as well as in the maintenance of symbiosis.

Key words: cell division, DNA damage and repair, genotoxic agents, Kinetoplast Associated Protein (KAPs), kDNA, symbiont-bearing trypanosomatids.

Introduction

The kinetoplast contains the mitochondrial DNA (kDNA) of trypanosomatids, which is arranged in a network of several thousand minicircles categorized into different classes and several dozen maxicircles that are virtually identical. Minicircles (0.5 - 10 kb) are physically connected to each other and also to maxicircles (20 - 40 kb) that are usually interwoven into the network periphery[1,2]. Maxicircle sequences encode components of the respiratory chain and ribosomal proteins, but first, posttranscriptional editing of the generated mRNA is required. This process is mediated in part by small noncoding guide RNAs (gRNAs) that are transcribed from minicircles[3,4]. The kDNA network is linked to the basal body through proteins that compose the tripartite attachment complex (TAC)[5]. Usually, loss of kDNA is associated with mitochondrial dysfunction, which makes this structure a potential chemotherapy target and diagnostic marker for trypanosomiasis[6,7,8].

In contrast to most eukaryotes, mitochondrial DNA replication in trypanosomatids is regulated during the cell cycle, initiating immediately before nuclear DNA replication in S phase followed by network scission and kinetoplast division during the G2 phase. The duplication cycle of the kinetoplast occurs in four steps: kDNA synthesis; scission, when kDNA is cleaved into two networks; separation; and partitioning of kinetoplast between the daughter cells during cytokinesis[9]. The kDNA network replication is a complex and unusual mechanism that involves various enzymes, such as the mitochondrial topoisomerase II (mtTopo II), which detaches covalently closed minicircles from the network. Minicircle replication initiates at the kinetoflagellar zone (KFZ), which comprises the region between the kDNA facing the basal body and the inner mitochondrial membrane. At the KFZ, the minicircles duplicate as theta structures, by UMSBP, Pol 1B, and other proteins and subsequently migrate to the antipodal sites. At this kinetoplast region, a primase enables the synthesis initiation of new DNA fragments following kDNA replication that involves more than 100 enzymes, such as universal minicircle sequence-binding protein (UMSBP) and polymerases. Next, each newly replicated minicircle is reattached to the network by the mtTopoII, maintaining at least one nick/gap that is filled by proteins, such as Pol β-PAK and DNA ligase kα, prior to the network scission. Later, the duplicated network is separated by the basal body distance, since the kDNA is connected to it via the TAC structure. This minicircle replication model was primarily based on findings obtained with *Trypanosoma brucei* and *Crithidia fasciculata*[4].

The kDNA arrangement varies according to species and developmental stages, ranging from densely packed fibers to a looser distribution in the kinetoplast matrix[10,11,12]. The proteins involved in this intriguing phenomenon have not been fully characterized. Kinetoplast-associated proteins (KAPs) are homologous to small basic histone H1-like proteins and nonhistone high-mobility group (HMG) box-containing proteins. KAPs have low molecular weights, are highly basic, are rich in alanine and lysine residues and contain a cleavable nine amino acid presequence involved in protein import to the kinetoplast in their amino-terminal region[13]. KAPs are involved in kDNA duplication, transcription, packing and topological remodeling[14,15,16]. KAPs can also bind to other proteins, such as UMSBP; in this case, they promote kDNA unpacking and facilitate the access of mtTopoII, which liberates minicircles from the network for replication[17].

The first model used to study the roles played by KAPs was the monoxenic *Crithidia fasciculata*, where the disruption of the *KAP1* gene generated viable cells with a phenotype of highly condensed kDNA fibers, which was similar to that observed when trypanosomatids were treated with nalidixic acid, an inhibitor of prokaryote topoisomerase II[15,18]. When both *C. fasciculata* alleles for *KAP2* and *KAP3* were disrupted separately, no detectable phenotypes were generated, and the same lack of phenotypes was observed to heterozygous cells (*kap2/3*$^{+/-}$), indicating a redundant function for these two encoded proteins. However, the double-knockout cells had notably slow proliferation, atypical cell morphology, an increased copy number of mRNAs encoding for ATPase and a significantly reduced respiration[15]. These first findings obtained with knockout cells indicated that KAPs were involved in distinct functions, such as kDNA arrangement and metabolism. Deletion of the *KAP3* gene was also performed in *Trypanosoma cruzi* by homologous recombination. Such null mutants did not exhibit changes in cell proliferation, differentiation, kDNA arrangement and infectivity, suggesting that this KAP is not essential for this parasite[19]. Later, the RNAi system was used to knockdown proteins associated with kDNA in *Trypanosoma brucei*. Downregulation of KAP6 promoted cell growth arrest and inhibition of covalently closed minicircle release, resulting in loss, shrinkage and disorganization of kDNA[20].

Symbiont-harboring trypanosomatids (SHTs), such as *Angomonas deanei* (previously classified as *Crithidia deanei*[21]), coevolve in a mutualist relationship with a single bacterium that divides in synchronicity with other host cell structures and is usually observed close to the nucleus. During the protozoan cell cycle, the bacterium is the first

DNA-containing structure to divide, followed by the kinetoplast and the nucleus[22,23,24]. The symbiont is a gram-negative of the Alcaligenaceae family that contains a reduced genome, is enclosed by two membranes and has a very reduced peptidoglycan layer[25,26,27]. Such species has been used to study the kinetoplast which, in these cells, presents atypical shapes and a looser kDNA arrangement, which is more susceptible to topoisomerase inhibitors and DNA-binding drugs[11,18,28,29]. Recently, phylogenetic analysis showed that SHTs present an expanded repertoire of nuclear encoded KAPs and that genes for KAP4 and KAP7 are present in all trypanosomatid species analyzed to date[11].

While mitochondrial DNA is subjected to the same damage sources as nuclear DNA, the reactive oxygen species (ROS) generated by the oxidative phosphorylation metabolism usually results in higher mutation rates in the mtDNA than does damage caused to nuclear DNA. In mammalian cells, base excision repair has been described as a restoration mechanism in the mitochondrion with the identification of several glycosylases, such as MYH, NEIL1, NEIL2 and UNG1, that are involved in the response of mtDNA to oxidative damage[30,31,32,33]. Other proteins, such as APE1, APE2, FEN1, and DNA2, were also detected, suggesting that all steps of this repair mechanism are present in the mitochondria of mammalians[34,35,36,37,38]. Mismatch removal activity was also identified in this organelle [39], although it has not been determined which proteins are involved in this process and whether the same pathway is active in the nucleus. However, the most striking and unexpected feature in mammalian cells is the lack of DNA repair mechanisms to address UV- and cisplatin-induced lesions on the mtDNA[40-42].

In trypanosomatids, some proteins involved in DNA repair have been described in both nuclear DNA and in kDNA metabolism. It was demonstrated that *T. cruzi* is able to remove oxidative lesions from both genomes, although damage to the kDNA remains higher than that in the nucleus[43,44,45]. This parasite contains DNA glycosylases that participate in the kDNA damage response[43-44], as well as polymerases involved in the response to oxidative stress, such as Polβ, Polβ-PAK [46,47] and Polκ, which are able to interact with intermediates of the homologous recombination[48]. Studies in *T. brucei* showed that the bloodstream form is able to deal with damage caused by cisplatin, hydrogen peroxide and methylmethanesulfonate (MMS), suggesting that DNA repair pathways are present in the parasite mitochondrion and that TbRad51 might be crucial to the response to alkylation lesions[49].

In the present work, for the first time, we used the CRISPR-Cas9 system to analyze the role played by KAP in a trypanosomatid protozoan. The results demonstrated that *A. deanei* Δ*kap4* mutants have reduced proliferation and exhibit morphological and ultrastructural alterations. In KAP4 mutants, the kDNA network becomes highly packed and cells have atypical phenotypes including filamentous bacterium and atypical numbers arrangement of nuclei and kinetoplasts. Considering alterations in kDNA arrangement, gene deletion mutants were not more sensitive to cisplatin and UV treatment than wild-type protozoa, but these genotoxic agents interfered with cytokinesis in both cell types. Notably, cisplatin and UV lesions can be repaired in mitochondrial DNA, which suggests that there are unique DNA repair mechanisms in the trypanosomatid kinetoplast.

Material and Methods

Cell culture

The *Angomonas deanei* wild type (WT – ATCC 30255) strain was cultured in Warren´s medium[50] supplemented with 10% fetal bovine serum. Protists were maintained by weekly passages by inoculating 10% of an established cell culture in fresh medium. WT and T7RNAPol-SpCas9 cell lines were grown at 28 ˚C for 24 h and cells with single or double deletions to *kap4* genes were grown for 48 h, both cases corresponded to the protozoan exponential growth phase. After this growth period, cells were used in assays or stored at 4˚C.

Analysis of cell growth and viability

For the growth curve, the initial cell concentration was 1 x 10^6 cells/mL, and counts were made every 24 h up to 72 h. Cell density was determined by counting live protozoa in a flow cytometer, where cell size was evaluated by detection of forward scatter on an SSA detector in a BD Accuri C6 flow cytometer (Becton Dickinson Bioscience BDB, San Jose, CA, USA). The relative growth rate (μ, expressed as h-1) of the exponential phase was estimated by an exponential function $y = Ae^{Bx}$, considering the parameters of culture cell density (cells/mL) vs culture time (h) of each strain, when B=μ. Such graphics only considered the cell density from 0 h to 48 h of growth, which corresponds to the

exponential phase, when all assays in this study were performed. Cell duplication time (DT) was calculated according to the formula $DT = \frac{ln2}{\mu}$.

To test cell viability, 5×10^6 cells were washed once with filtered-sterilized PBS (phosphate-buffered saline) pH 7.2 and incubated for 10 min with 20 μg/mL propidium iodide (PI). After this step, 10,000 events per sample were collected, and the fluorescence was detected on an FL-2 filter (488/630). The percentages of viable and nonviable cells were determined using control assays of life and death, respectively. To check cell death, cells were fixed in 4% paraformaldehyde for 10 min, washed with PBS, pH 7.2 and subsequently incubated with propidium iodide (PI 1:100). To control for living cells, protozoa were washed in PBS, pH 7.2, but were not incubated with PI. Cell fluorescence was detected as previously described. In such viability assays, as well as in growth curves, cells were collected on a BD Accuri C6 flow cytometer (Becton Dickinson Bioscience BDB, San Jose, CA, USA) using the manufacturer software.

Genotoxic treatment

WT and AdKAP4 mutants were compared by plating $1x10^7$ cells.mL^{-1} in the presence or absence of genotoxic agents. For cisplatin treatment, cells were incubated with 150 and 300 μM of the inhibitor for 1 h, washed three times with PBS at pH7.2 and resuspended in fresh medium. UVC irradiation (254 nm) was performed with a germicidal lamp at a fluence rate of 1,500 μJ/cm^2 (GS GeneLinker UV Chamber, Bio-Rad). For growth curves, in all conditions, the number of surviving cells was determined at 0 h (immediately before the treatment) and after 12 and 24 h of treatment, which corresponds to the *A. deanei* exponential phase[19]. Experiments were performed in triplicate. The cell number was determined in a hemocytometer chamber using the erythrosine vital stain (0.4% diluted in 1x PBS) to differentiate living and dead cells. Only dead cells were stained, presenting a red color. The survival rate was calculated by comparing treated and control cells, which were employed as references (considered as 100%).

Cell cycle analysis by flow cytometry

Protozoa were treated with cisplatin 150 and 300 μM for 1 h. Next, the cells were washed twice with PBS, pH 7.2, and the culture medium was replaced as described above.

Protozoa were analyzed before treatment, as well as 1 h and 24 h after the incubation with the inhibitor. Approximately 5×10^6 cells were pelleted, washed once with PBS and fixed in 0.25% paraformaldehyde at room temperature for 5 min. Next, the cells were permeabilized in 70% ethanol, in an ice bath, for 30 min and incubated with 100 µg/mL RNase and 25 µg/mL propidium iodide at 37 ˚C for 30 min. After this step, 10,000 events per sample were collected, and the fluorescence was detected on an FL-2 filter (488/630) on a BD Accuri C6 flow cytometer (Becton Dickinson Bioscience BDB, San Jose, CA, USA) using the manufacturer's software. DNA histograms were analyzed with the same software.

CRISPR-Cas9 gene editing

a - Protozoa transformation

Angomonas deanei transfections were performed by electroporation using the Amaxa 2B system program U-033 (Human T Cell Nucleofector™ Kit - Lonza), as previously described[24]. Cultures were immediately split into 2 populations, and recovered for 4 hours at 26 ºC before the addition of suitable antibiotics. Motile cells in both populations were counted and diluted for distribution in 96-well plates (200 µL of 1 or 0.5 cells/well). Clones were recovered after 5-8 days. *Angomonas deanei* T7RNAPol-SpCas9 was engineered using the pTB007 plasmid previously employed for *Leishmania* species, and SpCas9 expression was confirmed by Western blotting as in Beneke et al., 2017[51]. Transgenic lines were maintained in the following antibiotics and respective concentrations: G418 (250 µg. mL^{-1}) and hygromycin (300 µg. mL^{-1}).

b - CRISPR-Cas9 DNA fragment preparation

CRISPR-facilitated mutants were obtained by transfection of PCR fragments. The sgRNA sequence was obtained from EuPaGDT[52], selected based on correct on-target sequence (ADEAN_000063100)[53] and fewer *A. deanei* genome off-target hits, as well as sgRNA predicted activity. The sgRNA forward oligonucleotide is designed by flanking it with the T7RNAPol promoter (upstream) and the first 20 nucleotides of the SpCas9 scaffold (downstream). This oligo is combined with a universal primer containing the remaining sequence of SpCas9 backbone (OL00 - Table 1). Amplification was performed

in 20 µL using 0.2 mM dNTPs, 2 µM of each primer in Q5 reaction buffer and high-fidelity polymerase (NEB). The PCR program was set as 30 s at 98 °C followed by 35 cycles of 10 s at 98 °C, 30 s at 60 °C, and 15 s at 72 °C. The repair template fragments were produced using primers containing annealing sequences compatible with pPLOT and pT plasmids[51] and 30 nucleotide homology arms at the 5'end of the oligonucleotide, both forward and reverse, for recombination upstream and downstream of the DNA double strand break (DSB), respectively, at the UTR of the gene. Fragments were amplified from 20 ng of pTNeo_v1[51] using the same reaction buffer described above for sgRNA fragments in a final volume of 40 µL. PCR program was 10 min at 98 °C followed by 40 cycles of 30 s at 98 °C, 30 s at 60 °C, 2 min 15 s at 72 °C, and a final elongation step of 10 min at 72 °C. Products were run on 2% (sgRNAs) or 1% (repair templates) agarose gels in 0.5% Tris-Borate-EDTA (TBE) to confirm fragment amplification and expected sizes. Primer sequences are detailed in Table 1. DNA for transfection was prepared by combining sgRNA and repair templates followed by precipitation in a one-tenth volume of 3 M NaOAc, pH 5.5 and 2.5 volumes of ice-cold absolute ethanol and washing in 70% ethanol thereafter. DNA was resuspended in 10 µL of molecular biology grade water and immediately transfected.

Diagnostic PCRs

Genomic DNA (gDNA) was purified after clone cell culture amplification and kept under antibiotic selection, using the DNeasy Blood & Tissue Kit (Quiagen) following the manufacturer's instructions. PCRs were set using 50 ng of gDNA using PCRBIO HS Taq Mix Red (PCR Biosystems) and 0.4 µM of primers to amplify the CDS locus or the integrated repair template containing the resistance marker gene (Neo). The oligonucleotides OL05+OL6 were used to detect *KAP4* presence or absence, respectively. Oligonucleotides OL05+OL07 were used to confirm integration of the repair template containing the neomycin (Neo) resistance marker at *KAP4* loci. The PCR program used was 5 min at 95 °C followed by 25 cycles of 30 s at 95 °C, 30 s at 55 °C, 20 s at 72 °C and a final elongation step of 5 min at 72 °C. Reactions were directly run in a 0.8% agarose gel in TBE to confirm genetic manipulation by comparing the presence or absence of WT and mutants PCR products. Primer sequences are detailed in Table 1.

Fluorescence microscopy

a - DAPI Staining

Protozoa were collected by centrifugation at 2000 ×*g*, washed once with PBS (phosphate buffered saline) pH 7.4, fixed in 4% paraformaldehyde in the same solution, and mounted on poly-L-lysine-coated circular microscope coverslips (14 mm diameter), next, the slides were washed with PBS and incubated with 10 µg/ml 4′,6-diamidino- 2-phenylindole (DAPI, from Molecular Probes, Oregon, USA) for 10 min. After washing with PBS, slides were mounted using ProLong Gold (Molecular Probes), and visualized using a TCS SP5 confocal laser scanning microscope (Leica, Germany). Confocal images were obtained using an HCX PL APO 60× objective for light microscope oil immersion with a numerical aperture of 1.4. Optical sections obtained from the whole cell were transformed into 2D images by maximum projection in the manufacturer's software (LAS-X). The cellular patterns were determined by counting DNA-containing structures as nuclei, kinetoplasts and symbionts. Symbiont division was evaluated based on its form as described previously[22,24]. Analyses were based on counts of 1,000 cells of WT and KAP4 mutants.

b - Immunofluorescence with anti-porin antibody

Protozoa were washed in PBS and fixed with freshly prepared 2% formaldehyde diluted in PBS, for 1 h. After fixation, cells were adhered to poly-L-lysine-coated microscope coverslips and permeabilized with 4% Nonidet P-40 (NP-40) diluted in PBS for 45 min. Slides were incubated in blocking solution containing 1.5% bovine serum albumin (BSA), 0.5% teleostean gelatin (Sigma Aldrich), and 0.02% Tween 20 diluted in PBS. Next, slides were incubated for 1 h with antibody produced against the symbiont porin[54] diluted 1:10 in blocking solution. After that step, the cells were washed with PBS and incubated for 45 min with Alexa488-conjugated anti-mouse IgG (Molecular Probes, USA) diluted 1:200 in blocking solution. Slides were mounted using the anti-fading reagent ProLong Gold containing 5 µg. mL^{-1} of DAPI (4′,6-diamidino-2-phenylindole, MolecularProbes). Serial image stacks (0.36-µm Z-increment) were collected at 64x (oil immersion 1.4 NA) on an Elyra PS.1 microscope (Carl Zeiss) and three-dimensional projections were obtained on the Zen Black program (Carl Zeiss).

c - *In situ* labeling of kDNA networks

Cells were centrifuged, washed, and fixed in 2% paraformaldehyde diluted in PBS for 5 min. Next, cells were adhered to poly-L-lysine-coated slides for 10 min and washed twice in PBS containing 0.1 M glycine for 5 min. After permeabilization in methanol for 1 h at 20 °C, cells were rehydrated with three washes in PBS for 5 min and incubated for 60 min at room temperature in 25 µl of reaction solution containing: TdT reaction buffer (Roche Applied Science), 2.0 mM $CoCl_2$, 10 µM dATP, 2.5 µM Alexa Fluor 488-dUTP (Molecular Probes) and 10 units of TdT (Roche Applied Science). The reaction was stopped with three washes in 2xSSC for 5 min. Slides were mounted using the anti-fading reagent ProLong Gold containing 5 µg. mL^{-1} DAPI (4′,6-diamidino-2-phenylindole, MolecularProbes). Slides were examined on an Axiobserver microscope (Carl Zeiss), and images were collected at 100x (oil immersion 1.4 NA). Analyses were based on counts of 1,000 cells of WT and KAP4 mutants considering the kDNA replication as described by Liu and Englund (2007)[55].

Electron Microscopy

a - Scanning electron microscopy (SEM)

Sample processing was performed using glass coverslips precoated with 1 mg/mL poly-L-lysine. Protozoa were fixed for 1 h in 2.5% glutaraldehyde diluted in 0.1 M cacodylate buffer pH 7.2. Cells were subsequently adhered to coverslips, postfixed for 1 h with 1% osmium tetroxide diluted in cacodylate buffer, and dehydrated in a graded alcohol series (50%, 70%, 90%, and two exchanges of 100% ethanol for 10 min each step). Samples were critical-point dried in a Leica EM CPD030 apparatus (Leica, Wetzlar, Germany). Specimens were sputtered with gold in a Balzers FL9496 unit (Postfach 1000 FL-9496 Balzers Liechtenstein) and observed in an EVO 40 VP SEM (Zeiss, Germany). In all assays performed, approximately 500 cells were observed.

b - Transmission electron microscopy (TEM)

Protozoa were fixed for 1 h in 2.5% type II glutaraldehyde (Sigma, Missouri, USA) diluted in 0.1 M cacodylate buffer, pH 7.2. The protozoa were washed twice in cacodylate buffer and postfixed (1% osmium tetroxide, 0.8% potassium ferrocyanide, 5 mM calcium chloride diluted in 0.1 M cacodylate buffer) for 1 h. Samples were then washed in

cacodylate buffer, dehydrated in a graded series of acetone solutions (50%, 70%, 90%, and two exchanges of 100% acetone) for 10 min at each step, and embedded in Polybed resin. Ultrathin sections were stained with 5% uranyl acetate for 45 min and lead citrate for 5 min before observation in a Jeol 1200 EX TEM operating at 80 kV. In all assays performed, approximately 500 cells were analyzed.

Damage quantification by long-range qPCR analysis

Parasite cultures were treated with the respective drug as reported above. After treatment, $1x10^8$ cells were harvested by centrifugation at 3,000 *xg* for 5 min at the time points after treatment indicated on the graph. The first time point (0 h) was collected immediately after the end of UV radiation exposure, and after the washes to remove cisplatin from the media in cisplatin treatment. DNA extraction was performed by using the QIamp® DNA Mini and Blood Mini Kit (Qiagen, cat: 51104) protocol for tissue extraction.

Amplification was performed using a Kappa LongRange HotStart PCR Kit (Sigma, cat: KK3501). Specific primers for the mitochondrial coding region were used and are listed in Table 1. Amplification of the large mitochondrial fragment (approximately 10 kB) was performed by using primers qPCRMitF and qPCRMitR. Amplification of the small mitochondrial fragment (250 bp) was performed by using the primers qPCRMitSmF and qPCRMitR. For the nuclear fragment analyses, the amplification of the larger fragment was performed using the primers qPCRNucF and qPCRNucR. The smaller fragment was amplified using the primers qPCRNucSmF and qPCRNucR.

The assay consists of the comparison of the amount of amplified material of treated cells with the amount of amplified material within nontreated cells. The smaller fragment was used to normalize the amplification of the large fragments and to avoid any bias from uneven loading of template DNA among the various PCRs. The normalized value of treated and nontreated cells was compared, and the relative amplification was subsequently calculated. These values were used to estimate the average number of lesions/10 kb of the mitochondrial genome using a Poisson distribution. All the results presented are the mean of two technical replicates of amplification and two different biological experiments. Details of the data analysis can be found in the literature[56].

Results

To allow genetic manipulation in *A. deanei* facilitated by CRISPR-Cas9, we first generated an *A. deanei* mutant expressing SpCas9 and T7RNAPol by transfecting log-phase cells with the pTB007, generously provided by Dr. Eva Gluenz and previously used to generate a similar mutant in *Leishmania* sp.[52]. Western blotting confirmed SpCas9 expression in the mutants generated, using *L. mexicana* T7RNAPol-SpCas9 as a control (Supplementary Material 1).

To verify whether the expression of SpCas9 in the AdT7RNAPol-SpCas9 strain could constitutively cut nonspecific sites, long-range qPCR quantification was performed to determine the amount of possible accumulation of DNA damage in those cells. WT protozoa were used as a controls, since they do not contain the cassette construction for the SpCas9 expression. If SpCas9 generated nonspecific DNA damage, it was expected to produce a difference between the amplification ratio of the genetically modified strain in comparison with WT cells. The amplification for both strains was approxemetly 1, indicating that the expression of SpCas9 on *A. deanei* did not generate DNA strand breaks in a nonspecific manner in either nuclear or mitochondrial genomes (Figure 1, a and b). The confirmed mutant had a regular morphology, and SpCas9 expression was well tolerated. To delete *KAP4*, *A. deanei* was cotransfected with a repair template containing the neomycin resistance gene and 30 nt homologous to flanking *KAP4* UTRs', and 2 sgRNA templates were expressed *in vivo* by T7 RNA polymerase to insert DSBs at the 5' and 3' ends of the gene. Cells were kept under G418 pressure and mutants were confirmed by diagnostic PCR to detect the resistance cassette integration and *KAP4* deletion (Figure 1c). We were able to disrupt one or both alleles of *KAP4* by integrating a resistance marker (*NEO*), and enabling selection with neomycin (Figure 1d), thereby successfully validating our system.

Analyses of cell proliferation showed that WT, T7RNAPol-SpCas9 and *KAP4* mutants cultivated for 48 h, which corresponds to the peak of exponential phase, presented different proliferation profiles: when compared to WT protozoa, T7RNAPol-SpCas9 strain had a reduction of 19% in proliferation, whereas these values were equivalent to 67% and 69% to gene-deficient cells for one or both alleles of *KAP4*, respectively (Figure 1e). The duplication times of WT and T7RNAPol-SpCas9 were similar and equivalent to 7.1 and 7.4 h, respectively, whereas values obtained for Δ*kap4* with single or double deletions were 9.3 hours and 9.5 hours, respectively (Figure 1f). Although WT cells, as well as the T7RNAPol-SpCas9 background and *KAP4* mutants,

412 exhibited distinct decreases in proliferation after 48 h (Figure 1e), the viability rate after
413 72 h of cultivation was similar to that of all cell types, that is, approximately around 98.5%
414 (Figure 1g).

415 The morphological and ultrastructural analyses in this study used cells cultivated
416 for 24 h, which is equivalent to the exponential growth phase of *A. deanei,* whose
417 generation time is equivalent to 6 h. Transmission electron microscopy images showed
418 that as in other trypanosomatids, the nucleus usually occupies a central position in the cell
419 body and contains a nucleolus surrounded by heterochromatin, which is also observed at
420 the nuclear periphery. The symbiont was usually observed close to the host cell nucleus
421 and delimited by two membranes (Figure 2a). *A. deanei* WT displays a trapezoidal
422 kinetoplast containing a looser arrangement of the kDNA fibers in the central area and a
423 more densely packed array in the region that faces the TAC and connects the
424 mitochondrial DNA to the basal body (Figure 2b). This same phenotype was observed in
425 the CRISPR-Cas9 background cell line that did not have alterations in kinetoplast shape
426 or kDNA arrangement (Figure 2, d-e). Scanning electron microscopy demonstrated that
427 the WT and CRISPR-Cas9 background strains presented the typical choanomastigotes of
428 the *Angomonas* genus. The smooth cell surface often exhibited gentle undulations that
429 corresponded to mitochondrial branches (Figure 2, c-f).

430 In cells with a single deletion (*kap4*$^{+/-}$) the kinetoplast shape was maintained;
431 however, kDNA fibers of the central area were broken in most cells, and the kinetoplast
432 network was determined to be more condensed as a whole than those observed in control
433 cells. In some instances, the nucleus presented matrix loss and a more condensed
434 chromatin (Figure 2, g and i). Such protozoa showed unusually elongated symbionts,
435 indicating that bacterial division was impaired (Figure 2h). In *KAP4* null mutants, cells
436 with division impairment phenotype usually presented two flagella in the same flagellar
437 pocket (Figure 2m). The symbiotic bacterium was also affected in these cells, which
438 presented filamentous forms surrounded by small vacuoles (Figure 2n). The kDNA
439 packing was severely compromised in the whole network, especially in the central area
440 (Figure 2o). Alterations in the nuclear ultrastructure were rarely observed.

441 As a next step, analysis by scanning electron microscopy was performed by
442 comparing *KAP4* mutants and WT protozoa. Cells with a single gene deletion (*kap4*$^{+/-}$)
443 had alterations in morphology, with many protozoa showing a round shape with a
444 shortened flagellum (Figure 2j, white arrow). Part of the culture presented body shape

asymmetry during division (Figure 2j, gray arrow), which resulted in the generation of daughter cells with different dimensions (Figure 2k). Protozoa with multiple cell bodies and flagella were also observed, indicating cytokinesis impairment (Figure 2l). Null mutants also presented morphological alterations, such as cell body shortening and flagellar length reduction (Figure 2p). A high number of cells with impaired cytokinesis was observed, thereby generating a popcorn-like phenotype (Figure 2, q-r).

Analyses of cellular patterns were performed in *A. deanei* labeled with DAPI and with an anti-porin antibody that recognizes the endosymbiont, considering the number of nuclei, kinetoplasts and symbionts, as well as the shape of the bacterium (Figure 3). As expected, in asynchronous cultures of WT cells, approximately 30%, presented one rod-shaped symbiont, one kinetoplast and one nucleus (1S1K1N). Most cells, that is, approximately 50%, also presented 1S1K1N; however, the symbiont presented a constricted or dividing format. The other part of the culture, approxemetly 20%, was composed of cells containing two rod-shaped symbionts. Such protozoa presented one or two kinetoplasts and nuclei; however, kinetoplast division was always observed before the karyokinesis. In *KAP4* mutants cultivated for 24 h, protozoa presented atypical phenotypes as two nuclei, one kinetoplast and one filamentous symbiont (1Sf2N1K) or two nuclei, two kinetoplasts and one filamentous symbiont (1Sf2N2K), an indication of kDNA division and cytokinesis blockage, respectively (Figure 3, a-d). In KAP4 mutants cultivated for 24 h, filamentous symbionts were observed in 3% $kap4^{+/-}$ cells and in 54% of $kap4^{-/-}$ protozoa, exhibiting bacterium division impairment (Figure 3e).

The counting of cell patterns in KAP4 mutants showed that the percentage of filamentous symbionts was higher in cells containing one bacterium, one nucleus and one kinetoplast (1Sf1N1K) than in cells containing two nuclei or two kinetoplasts, indicating that as the cell cycle progresses, the symbiont filamentation increases, eventually leading to bacterial lysis. The percentage of cells containing one filamentous symbiont, two nuclei and one kinetoplast (1Sf2N1K) was almost three times higher than in $kap4^{-/-}$ protozoa when compared to $kap4^{+/-}$ cells, indicating that in the double mutant, kinetoplast division was more affected (Figure 3f). To check whether the KAP4 mutant phenotype has an impact on kDNA replication, assays of dUTP incorporation by the deoxynucleotidyl transferase terminal (TdT) were performed. The results showed that the percentage of cells with the kDNA in the early replication stage was 62.5% lower in cells containing deletions of both *KAP4* genes than in WT protozoa. During this stage, the kinetoplast

exhibits strong labeling in the antipodal sites but little labeling in the kDNA network (Figure 3g).

Considering the structural results obtained in this work, we assumed that *A. deanei* KAP4 could participate in kDNA metabolism. To confirm this hypothesis, WT and mutant cells were exposed to cisplatin or UV radiation to verify the cell response to DNA damage. These agents cause distortions in the DNA that can impair transcription and replication, with cisplatin lesions being more effective than UV light[48, 49, 50, 51,52]. Protozoa that had one or both *KAP4* genes deleted were able to grow after treatment with cisplatin or exposure to UV, although in cisplatin treatment, the mutant cells presented a slight decrease in cell proliferation compared to the WT strain after 12 hours of treatment, especially the single gene-deficient mutant treated with the highest inhibitor concentration (Figure 4, a-d).

Considering the cellular morphology and cellular organization, microscopy analyses were performed to test whether *KAP4* mutants presented atypical phenotypes in relation to WT cells after cisplatin treatment. This compound interacts with DNA and proteins and forms intrastrand or interstrand DNA crosslinks that cause distortions in the double helix, thereby blocking duplication and transcription. Transmission electron microscopy images showed that WT cells did not present nuclear or kinetoplast changes after incubation with cisplatin, even when a higher drug concentration (300 µM) was used (Figure 5, a-c). The same phenomenon was observed in the background T7RNAPol-SpCas9 cell line (data not shown). Similarly, *KAP4* mutants did not display topological rearrangement on the kDNA network compared to WT cells treated with cisplatin (Figure 5, h and m). However, other cellular structures suffered alterations in mutant protozoa. In *kap4*$^{+/-}$ cells, nuclear DNA unpacking was observed, as well as myelin figures in the cytoplasm (Figure 5f, black arrow) and mitochondrial swelling. The abundance of the endoplasmic reticulum was noted and also its frequent association with the symbiont, which sometimes was seen surrounded by this organelle, suggested an autophagic process (Figure 5f, arrowheads). The symbiont also displayed matrix loss and alterations in its DNA condensation (Figure 5g, white arrows). In null mutants treated with 300 µM cisplatin, the primary ultrastructural alteration was observed in the symbiont that presented membrane convolutions (Figure 5k, arrow), matrix loss and densely packed DNA fibers (Figure 5l, white arrows). It is also worthwhile to mention the presence of vacuoles around the symbiont, indicating that the bacterium had lysed (Figure 5, k-l).

Analyses by SEM showed that cultures of *A. deanei* WT cells presented a higher incidence of rounded protozoa with a shortening flagellum after treatment with 150 and 300 µM cisplatin for 24 h (Figure 5, d-e). This phenotype was also observed in mutant cells after treatment with both concentrations (Figure 5, i-j, n-o, white arrowheads). Protozoa presenting a fat cell-like phenotype and lacking the flagellum (Figure 5i, white arrow) were observed after treatment with 150 µM cisplatin for 24 h. After using 300 µM of this drug, protozoa with the cytokinesis phenotype were observed more frequently (Figure 5j), indicating division impairment, as well as plasma membrane blebs at the posterior end of the cell body (Figure 5o). Protozoa that had one allele deleted seemed to have their morphology more affected than null mutant when treated with this genotoxic agent.

Cells subjected to cisplatin treatment presented atypical phenotypes, as demontrated by fluorescence microscopy analysis. When treated with the lower inhibitor concentration (150 µM), WT trypanosomatids presented rounded shapes with a reduced flagellum length and the fat cell phenotype. Symbionts were seen in the filamentous format, presenting several nucleoids (Figure 6, a-a"). Mutants for *KAP4* treated with cisplatin also presented filamentous bacterium, but in this case, protozoa lacking the bacterium were also observed, as well as cells presenting two nuclei and one kinetoplast (Figure 6, b-b" and c-c"). Next, we counted the number of protozoa containing a filamentous bacterium after cisplatin treatment for 24 h. In WT *A. deanei,* filamentous bacteria were not identified in non-treated cells, as previously demonstrated. However, after incubation with 150 µM and 300 µM of cisplatin, 14% and 3% of the cells showed filamentous symbionts, respectively. In *kap4*$^{+/-}$ protozoa, when both concentrations of cisplatin were used, the percentage of filamentous bacteria was similar, that is, approximately 2 %. In the null mutant (*kap4*$^{-/-}$), values were equivalent to 14% and 8%, respectively (Figure 6d).

These results indicate that treatment with cisplatin induced symbiont filamentation and that a higher concentration of the inhibitor (300 µM) augmented symbiont lysis, as also suggested by transmission electron microscopy data. Counting of cellular patterns demonstrated that after treatment with cisplatin, the highest percentage of bacterial filamentation was present in the double mutant cells containing one nucleus and one kinetoplast (1Fs1N1K). In these cells, the percentage of protozoa with a filamentous symbiont decreased in a concentration-dependent manner. The percentage of

protozoa with bacterial filamentation also decreased with the progression of the cell cycle, as in cells containing two nuclei, reinforcing the notion of the bacterial lysis. Taken together, these data indicate that somehow genotoxic agents alter the cell division pattern in *A. deanei* and that this effect is exacerbated in mutant cells (Figure 6e). Cisplatin can block replication and trigger checkpoints at the end of S phase and the beginning of G2 to repair lesions, thereby causing cell cycle arrest. However, when cells treated with cisplatin were submitted to flow cytometry analysis, they did not show cell cycle alterations in relation to control cells, even after treatment with 300 µM for 24 h (Supplementary Figure 2).

The susceptibility of WT and mutant cells to UV radiation was also verified. Thus, protozoa were subjected to UV-C irradiation, which affects the DNA replication and transcription and can be repaired by nucleotide excision. Ultrastructural and morphological analyses were performed after 24 h of protozoa irradiation at 1500 µJ/m2. The results obtained by transmission electron microcopy were similar to those observed for WT and *KAP4* mutant cells treated with cisplatin: nuclear DNA and kDNA did not suffer additional topological alterations in relation to nonirradiated cells (Figure 7, a-b, f-g, and k), and a close association of the ER with the symbiont occurred frequently, strongly indicating autophagy (Figure 7, a, f, and k, white arrowheads). Notably, after irradiation, mutant cells presented bacteria with a higher DNA condensation (Figure 7, a, g, and k, white arrows). Furthermore, polynucleated cells were observed (Figure 7l).

Scanning electron microscopy analyses showed that WT protozoa suffered morphological alterations after irradiation, exhibiting wrinkled cell surfaces and irregular forms that indicated cytokinesis impairment (Figure 7, c-e). In single- and double-*KAP4*-deleted mutants, the morphological modifications were exacerbated: many protozoa presented multiple interconnected cell bodies, reinforcing the notion that cytokinesis was blocked (Figure 7, h-i). Such cells also presented wrinkled surfaces, and the flagellum was absent in some instances (Figure 7, h and j, white arrows), as also observed in null mutants (Figure 7, m and o, white arrows). In this last case, a high number of round cells were also observed (Figure 7, m-o).

Irradiated protozoa were also labeled with DAPI, exhibiting atypical phenotypes that were compatible with asymmetric division and cytokinesis impairment, such as the presence of one kinetoplast and two nuclei in cells containing two symbionts (Figure 8a) and dyskinetoplastic cells. Such morphotypes were observed in WT cells, as well as in

mutant cells (Figure 8b). Protozoa with filamentous bacterium were observed more frequently in WT cells than in *KAP4* mutants, on which symbiont division was probably more strongly affected. The absence of the symbiont was observed in null mutants (Figure 8c), which may have been related to the possible occurrence of autophagy, in this case, a symbiophagy, that generated aposymbiotic cells, as suggested by transmission electron microscopy. The very reduced number of WT cells presenting filamentous symbionts (1.4%) and the absence of this phenotype in mutant cells reinforced this notion (Figure 8d). The percentage of irradiated protozoa presenting atypical phenotypes was low in all cell types (Figure 8e).

To verify whether *KAP4* was involved in kDNA repair, mutant and wild-type cells of *A. deanei* cells were treated with cisplatin and UV radiation, as described before, and DNA repair kinetics were measured by long-range qPCR assay. After treatment with 300 μM cisplatin, WT and both mutant strains presented the same levels of DNA damage on the kDNA, which was approximately 1.5 lesions/10 kB. The repair kinetics were very similar for all cell types: after 3 h of treatment, levels of kDNA damage were almost undetectable, reaching the slowest point after 6 h (Figure 9 a-b, Supplementary Material 3). A similar phenotype was observed for the UV radiation. The levels and DNA repair kinetics of mutant cells were very similar to those observed in WT cells. After 1 h of treatment, most damage had already been repaired, although it required 3 h after UV radiation to reach the same level of repair that was observed in cisplatin-treated cells, with the lowest point being observed at 6 h (Figure 9, c-d). Taken together, these results demonstrate that *KAP4* was not directly involved in the removal of DNA damage generated by cisplatin and UV radiation but, notably, show that lesions generated by both genotoxic agents could be repaired in mitochondrial DNA (Figure 9, a-d).

Discussion

In recent decades, *A. deanei* has been used as a model for endosymbiosis and the origin of organelles. Genome sequencing is available[26,27,62], and molecular tools for gene function studies were developed, although with limited use on studies of genes essentially and symbiosis maintenance[24,63]. The recent application of highly efficient CRISPR-Cas9 protocols to other trypanosomatids, such as *Leishmania* and *T. cruzi*, accelerated functional studies with gene deletion[51,63,64]. In this study, for the first time, we describe

gene depletion in an endosymbiont-harboring trypanosomatid. Phylogenetic proximity with *Leishmania* enabled the successful application of the CRISPR-Cas9 system developed by Beneke and colleagues (2017)[51] to *A. deanei*, resulting in efficient deletion of *KAP4*, a kinetoplast associated protein present in all trypanosomatids so far analyzed[9].

KAPs can neutralize the negative DNA charge, thus facilitating the interaction of mitochondrial proteins with kDNA, as those involved in replication and transcription. In this work, deletion of *A. deanei KAP4* generated trypanosomatids with reduced cell proliferation and generated cells with atypical phenotypes, as those presenting two nuclei and one kinetoplast, as well as cytokinesis impairment. Cells containing aberrant numbers of nucleus and kinetoplast were also observed in null mutants of *C. fasciculata* for *KAP2* and *KAP3* that presented cell division block[16]. In *T. brucei*, the RNAi knockdown of a kDNA associated protein, resulted in reduced growth and in the appearance of dyskinetoplastic cells[64]. These results reinforce the importance of KAPs to cell proliferation and kDNA network replication in order to guarantee that each new protozoa will receive one kinetoplast during trypanosomatid division.

The coordinated division of the symbiont with the host cell nucleus was previously demonstrated in *A. deanei* and in *Strigomonas culicis*, another symbiont-harboring trypanosomatid[22-24]. In the present work, it was interesting to observe in *KAP4* mutant cells that the kDNA condensation, which is associated with kinetoplast replication impediment, resulted in symbiont filamentation. This filamentation occurred most frequently in mutant with two nuclei and one kinetoplast. Consistent with this notion, TdT labeling showed a lower percentage of *kap4*$^{-/-}$ cells in the early replication phase when compared to the WT protozoa, indicating that in such cells the mitochondrial DNA replication was delayed or even impaired. Since kDNA loss resulting in dyskinetoplastic protozoa was not observed, it can be assumed that the impediment of mitochondrion DNA replication promoted cytokinesis blockage. Taken together, the results indicate that bacterial division is also coordinated with kinetoplast replication, but further studies are essential to confirm this hypothesis. Cell cycle checkpoints are not well established for most trypanosomatids species, nor are the factors that coordinate the equal partitioning of single copy organelles to daughter cells. Such questions are best studied in *T. brucei*, especially by investigating the role of protein kinases in cell cycle progression, organelle positioning and protozoan morphology[66,67,68,69]. Recently, it was shown that *T. brucei* UMSBP2, which is involved in kDNA replication and segregation, is also localized at

642 telomeres. The RNAi system showed that this protein not only participates in nuclear
643 division but also plays a role in the coordinated replication of DNA-containing
644 organelles[70].

645 In *A. deanei KAP4* mutants, the high level of kDNA packing was associated with a
646 delay in cell proliferation and a delay of kDNA replication at the early stage, when the
647 covalently closed minicircles are released from the network to initiate replication into the
648 KFZ and then migrate to antipodal sites, where this process continues[4]. Previously, it was
649 shown that the downmodulation of *T. brucei* P93, a kDNA-associated protein localized
650 in antipodal sites, resulted in loss of gapped minicircles and consequently in the network
651 reduction[71]. Similarly, in TbKAP6 RNAi cells, the levels of total minicircles and
652 maxicircles decreased the total amount of nicked/gapped minicircles. In such cells, the
653 kinetoplast presented network shrinkage or elongation, but in both cases, two basal bodies
654 could be identified, indicating failures in kDNA replication and scission. Conversely,
655 protozoa overexpressing TbKAP6 minicircle decatenation were enhanced, indicating that
656 a controlled expression of this protein is required for proper kDNA replication[20].

657 The kDNA arrangement and metabolism are the result of the coordinated activity
658 of a set of mitochondrial proteins that serve different functions. In addition to KAPs, other
659 proteins are involved in the kDNA replication, such as the minicircle replication factor
660 (MiRF172), which is supposedly involved in the reattachment of replicated minicircles
661 to the kDNA disc. Once depleted, *T. brucei* cells presented reduced kDNA content or
662 even a dyskinetoplastic phenotype[72]. Downregulation of mitochondrial heat shock
663 proteins 70 and 40 also showed impairment of minicircle replication and loss of kDNA,
664 demonstrating the importance of chaperones to the maintenance of the kinetoplast as a
665 cellular structure[73]. In the present work, the generation of dyskinetoplastic cells was not
666 observed among KAP4 mutants. Although the gene deletion promoted increased kDNA
667 compaction, the data obtained by qPCR did not indicate loss of mitochondrial DNA. In
668 UV-irradiated protozoa, a very low percentage of cells without a kinetoplasts was
669 observed.

670 The DNA repair kinetics showed no differences between *KAP4* mutant cells and
671 the WT strain. In both cases, protozoa were able to efficiently repair the damage generated
672 by cisplatin and UV radiation. In addition, differences in the long-term survival of these
673 cells were not observed. For both genotoxic agent treatments, the kDNA accumulated the
674 same amounts of lesions in WT or *KAP4* mutant cells, suggesting that the topological

675 alterations observed in the kinetoplast network did not affect the susceptibility to DNA
676 damage. It is well established that damage generated by UV radiation and cisplatin is not
677 repaired in humans and other mammalian cells[40,41]. Notably, in *A. deanei*, damage caused
678 by both genotoxic agents on the kDNA was repaired, representing the first demonstration
679 of this type of repair in mitochondrial DNA. The repair kinetics observed in this instance
680 are not related to the kDNA loss, since the number of dyskinetoplastic cells after
681 genotoxic treatment is negligible.

682 Notably, the DNA repair kinetics were very similar when cisplatin was tested in
683 WT and mutant cells, and the same phenomenon was observed for UV radiation.
684 However, accentuated differences were observed when comparing the two treatments:
685 DNA repair by cisplatin was very fast; thus, after 1 h, most lesions were already repaired,
686 whereas for UV radiation damage, the kinetic is slower. Although it is described that
687 lesions caused by UV and cisplatin are mainly repaired by the nucleotide excision repair
688 pathway, the kinetics observed in this work strongly suggest that lesions caused by each
689 genotoxic treatment activated different and specific responses in *A. deanei*. It is well-
690 known that lesions that block transcription are repaired very quickly compared to other
691 types of lesions. It has also been also reported that the main lesion caused by UV light
692 (thymine dimers) can be tolerated by RNA polymerase[74,75]. In trypanosomatids that
693 present a single mitochondrion, it is possible that a DNA repair pathway associated with
694 transcription exists. The repair of UV lesions may also be associated with the
695 recombination process. In *T. brucei*, it was seen that cells deficient in the Rad51 gene are
696 not able to adequately repair lesions caused by methyl methanesulfonate (MMS)[49,76,77].

697 Our structural analyses using microscopy techniques showed distinct atypical
698 phenotypes after treatment with cisplatin or ultraviolet radiation. This phenomenon may
699 be observed because cisplatin can cause more toxic injuries that culminate in cell death.
700 Accordingly, mutant protozoa have higher sensitivity to elevated concentrations of
701 cisplatin and lower percentages of cells containing duplicated nuclei and kinetoplasts than
702 WT or UV-irradiated cells. In mutant cells, this inhibitor promoted a decrease in
703 proliferation and in the number of filamentous symbionts, indicating bacterium lysis.
704 Notably, the cell morphology and growth of KAP4 single allele deletion mutants were
705 more affected by high doses of cisplatin than those of the null mutant cells. Since KAP4
706 is not an essential protein, it cannot be ruled out that an adaptation process has occurred
707 in cells where both copies of the genes were deleted. A similar phenomenon was observed

in null mutants of *Trypanosoma cruzi* and *Trypanosoma brucei* for the MSH2 gene, which encodes a central component of the eukaryotic DNA mismatch repair (MMR) pathway[78].

In this work, we demonstrated for the first time that the CRISPR-Cas9 system can be used with success to delete genes in *A. deanei*. KAP4 is not an essential protein, but it is involved in the kDNA compaction, leading to the appearance of cells with atypical phenotypes, such as symbiont filamentation and the appearance of two nuclei and one kinetoplast. This protein does not seem to participate in the mitochondrial DNA repair process; however, lesions caused by cisplatin and UV radiation are repaired in the kDNA of this protozoan. The repair kinetics are different for each genotoxic agent, indicating that different pathways are used to repair the lesions. In the case of cisplatin, repair may be associated with transcription.

References

1. Lukes J, *et al*. Kinetoplast DNA Network: Evolution of an Improbable Structure *Eukaryot Cell*. **1**(4): 495–502. https://doi.org/10.1128/ec.1.4.495-502.2002 (2002)
2. Hajduk SL, Klein VA, Englund PT. Replication of kinetoplast DNA maxicircles. *Cell* **36**(2), 483–492. https://doi.org/10.1016/0092-8674(84)90241-1 (1984)
3. Hajduk S & Ochsenreiter T. RNA editing in kinetoplastids. *RNA Biol*. **7**(2):229-236. https://doi:10.4161/rna.7.2.11393 (2010).
4. Jensen, R. E., & Englund, P. T. Network news: the replication of kinetoplast DNA. *Annu. Rev. Microbiol.* **66**, 473–491. https://doi.org/10.1146/annurev-micro-092611-150057 (2012).
5. Ogbadoyi, E. O., Robinson, D. R. & Gull, K. A high-order trans-membrane structural linkage is responsible for mitochondrial genome positioning and segregation by flagellar basal bodies in trypanosomes. *Molecular biology of the cell*, **14**(5), 1769–1779. https://doi.org/10.1091/mbc.e02-08-0525 (2003).
6. Tittawella I. Kinetoplast-associated proteins as potential drug targets and diagnostic markers for trypanosomiasis. *The Journal of infection*, **29**(3), 359–361. https://doi.org/10.1016/s0163-4453(94)91496-6 (1994).
7. Mukherjee, S. *et al.* Metabolic Inhibitors as Antiparasitic Drugs: Pharmacological, Biochemical and Molecular Perspectives. *Current drug metabolism*, **17**(10), 937–970. https://doi.org/10.2174/1389200217666161004143152 (2016).
8. Menna-Barreto, R. F. & de Castro, S. L. Clear Shot at Primary Aim: Susceptibility of *Trypanosoma cruzi* Organelles, Structures and Molecular Targets to Drug

Treatment. *Curr. Top. Med. Chem.* **17**(10), 1212–1234. https://doi.org/10.2174/1568026616666161025161858 (2017).

9. Mensa-Wilmot, K. *et al.* Kinetoplast Division Factors in a Trypanosome. Trends Parasitol., **35**(2), 119–128. https://doi.org/10.1016/j.pt.2018.11.002 (2019).
10. De Souza W.Basic cell biology of *Trypanosoma cruzi*. *Curr. Pharm. Des.,* **8**(4), 269–285. https://doi.org/10.2174/1381612023396276 (2002).
11. de Souza, S. *et al.* Expanded repertoire of kinetoplast associated proteins and unique mitochondrial DNA arrangement of symbiont-bearing trypanosomatids. *PloS one*, **12**(11), e0187516. https://doi.org/10.1371/journal.pone.0187516 (2017).
12. Gonçalves, C. S. *et al*. Revisiting the *Trypanosoma cruzi* metacyclogenesis: morphological and ultrastructural analyses during cell differentiation. *Parasit Vectors*, **11**(1), 83. https://doi.org/10.1186/s13071-018-2664-4 (2018).
13. Xu, C. W. *et al*. Nucleus-encoded histone H1-like proteins are associated with kinetoplast DNA in the trypanosomatid *Crithidia fasciculata*. *Mol. Cell. Biol.,* **16**(2), 564–576. https://doi.org/10.1128/mcb.16.2.564 (1996).
14. Xu, C. & Ray, D. S. Isolation of proteins associated with kinetoplast DNA networks in vivo. *Proc Natl Acad Sci USA*, **90**(5), 1786–1789. https://doi.org/10.1073/pnas.90.5.1786 (1993).
15. Lukes, J. *et al*. Disruption of the *Crithidia fasciculata* KAP1 gene results in structural rearrangement of the kinetoplast disc. *Mol Biochem Parasitol*, **117**(2), 179–186. https://doi.org/10.1016/s0166-6851(01)00348-6 (2001).
16. Avliyakulov, N. K., Lukes, J., & Ray, D. S. Mitochondrial histone-like DNA-binding proteins are essential for normal cell growth and mitochondrial function in *Crithidia fasciculata*. *Eukaryotic cell*, ***3***(2), 518–526. https://doi.org/10.1128/ec.3.2.518-526.2004 (2004).
17. Kapeller, I., Milman, N., Yaffe, N., & Shlomai, J. Interactions of a replication initiator with histone H1-like proteins remodel the condensed mitochondrial genome. *J. Biol. Chem*, **286**(47), 40566–40574. https://doi.org/10.1074/jbc.M111.270322 (2011).
18. Cavalcanti, D. P. *et al*. The effect of topoisomerase II inhibitors on the kinetoplast ultrastructure. *Parasitol. Res*. **94**(6), 439–448. https://doi.org/10.1007/s00436-004-1223-4 (2004).
19. de Souza, F. S. *et al*. Knockout of the gene encoding the kinetoplast-associated protein 3 (KAP3) in *Trypanosoma cruzi*: effect on kinetoplast organization, cell proliferation

and differentiation. *Mol Biochem Parasitol*, **172**(2), 90–98. https://doi.org/10.1016/j.molbiopara.2010.03.014 (2010).

20. Wang, J., Pappas-Brown, V., Englund, P. T., & Jensen, R. E.TbKAP6, a mitochondrial HMG box-containing protein in *Trypanosoma brucei*, is the first trypanosomatid kinetoplast-associated protein essential for kinetoplast DNA replication and maintenance. *Eukaryotic cell*, **13**(7), 919–932. https://doi.org/10.1128/EC.00260-13 (2014).
21. Teixeira, M.M *et al*. Phylogenetic validation of the genera *Angomonas* and *Strigomonas* of trypanosomatids harboring bacterial endosymbionts with the description of new species of trypanosomatids and of proteobacterial symbionts. *Protist.* **162**(3): 503-524. https://doi.org/10.1016/j.protis.2011.01.001 (2011)
22. Motta, M. C. *et al*. The bacterium endosymbiont of *Crithidia deanei* undergoes coordinated division with the host cell nucleus. *PloS one*, **5**(8), e12415. https://doi.org/10.1371/journal.pone.0012415 (2010).
23. Brum, F. L. *et al*. Structural characterization of the cell division cycle in *Strigomonas culicis*, an endosymbiont-bearing trypanosomatid. *Microsc Microanal*. **20**(1), 228–237. https://doi.org/10.1017/S1431927613013925 (2014).
24. Catta-Preta, C. M. *et al*. Endosymbiosis in trypanosomatid protozoa: the bacterium division is controlled during the host cell cycle. *Front Microbiol*, 6, 520. https://doi.org/10.3389/fmicb.2015.00520 (2015).
25. Motta, M.C.M. *et al*. Detection of penicillin binding proteins in the endosymbiont of the trypanosomatid *Crithidia deanei*. J. Eukaryotic Microbiol. **44**: 492-496 (1997a).
26. Alves, J. M. *et al*. Genome evolution and phylogenomic analysis of Candidatus Kinetoplastibacterium, the betaproteobacterial endosymbionts of *Strigomonas* and *Angomonas*. Genome Biol. Evol, ***5***(2), 338–350. https://doi.org/10.1093/gbe/evt012 (2013).
27. Motta, M. C. *et al*. Predicting the proteins of *Angomonas deanei*, *Strigomonas culicis* and their respective endosymbionts reveals new aspects of the trypanosomatidae family. *PloS one*, **8**(4), e60209. https://doi.org/10.1371/journal.pone.0060209 (2013).
28. Cavalcanti, D. P., Thiry, M., de Souza, W. & Motta, M. C. The kinetoplast ultrastructural organization of endosymbiont-bearing trypanosomatids as revealed by deep-etching, cytochemical and immunocytochemical analysis. *Histochem Cell Biol*, **130**(6), 1177–1185. https://doi.org/10.1007/s00418-008-0450-7 (2008).

29. Zuma, A. A. *et al*. Effect of topoisomerase inhibitors and DNA-binding drugs on the cell proliferation and ultrastructure of *Trypanosoma cruzi*. *Int. J. Antimicrob.*, **37**(5), 449–456. https://doi.org/10.1016/j.ijantimicag.2010.11.031 (2011).
30. Chatterjee, A., & Singh, K. K. Uracil-DNA glycosylase-deficient yeast exhibit a mitochondrial mutator phenotype. *Nucleic acids research*, *29*(24), 4935–4940. https://doi.org/10.1093/nar/29.24.4935 (2001).
31. Nakabeppu Y. Regulation of intracellular localization of human MTH1, OGG1, and MYH proteins for repair of oxidative DNA damage. *Progress in nucleic acid research and molecular biology*, *68*, 75–94. https://doi.org/10.1016/s0079-6603(01)68091-7 (2001).
32. Takao, M., Zhang, Q. M., Yonei, S., & Yasui, A. Differential subcellular localization of human MutY homolog (hMYH) and the functional activity of adenine:8-oxoguanine DNA glycosylase. *Nucleic acids research*, *27*(18), 3638–3644. https://doi.org/10.1093/nar/27.18.3638 (1999).
33. Han, D. *et al.* NEIL1 and NEIL2 DNA glycosylases protect neural crest development against mitochondrial oxidative stress. *eLife*, *8*, e49044. https://doi.org/10.7554/eLife.49044 (2019).
34. Mitra, S., *et al.* Intracellular trafficking and regulation of mammalian AP-endonuclease 1 (APE1), an essential DNA repair protein. *DNA repair*, **6**(4), 461–469. https://doi.org/10.1016/j.dnarep.2006.10.010 (2007).
35. Tsuchimoto, D. *et al*. Human APE2 protein is mostly localized in the nuclei and to some extent in the mitochondria, while nuclear APE2 is partly associated with proliferating cell nuclear antigen. *Nucleic Acids Res*, **29**(11), 2349–2360. https://doi.org/10.1093/nar/29.11.2349 (2001)
36. Kalifa, L., Beutner, G., Phadnis, N., Sheu, S. S., & Sia, E. A. Evidence for a role of FEN1 in maintaining mitochondrial DNA integrity. *DNA repair*, ***8***(10), 1242–1249. https://doi.org/10.1016/j.dnarep.2009.07.008 (2009).
37. Kazak, L. *et al*. A cryptic targeting signal creates a mitochondrial FEN1 isoform with tailed R-Loop binding properties. *PloS one*, ***8***(5), e62340. https://doi.org/10.1371/journal.pone.0062340 (2013).
38. Zheng, L. *et al*. Human DNA2 is a mitochondrial nuclease/helicase for efficient processing of DNA replication and repair intermediates. *Molecular cell*, ***32***(3), 325–336. https://doi.org/10.1016/j.molcel.2008.09.024 (2008).

841 39. Mason, P. A., Matheson, E. C., Hall, A. G., & Lightowlers, R. N. Mismatch repair
842 activity in mammalian mitochondria. *Nucleic Acids Res*, **31**(3), 1052–1058.
843 https://doi.org/10.1093/nar/gkg167(2003).
844 40. Clayton, D. A., Doda, J. N., & Friedberg, E. C. The absence of a pyrimidine dimer
845 repair mechanism in mammalian mitochondria. *Proc Natl Acad Sci USA*, **71**(7),
846 2777–2781. https://doi.org/10.1073/pnas.71.7.2777 (1974).
847 41. Podratz, J. L. *et al*. Cisplatin induced mitochondrial DNA damage in dorsal root
848 ganglion neurons. *Neurobiol. Dis.*, **41**(3), 661–668.
849 https://doi.org/10.1016/j.nbd.2010.11.017 (2011).
850 42. Pascucci, B. *et al*. DNA repair of UV photoproducts and mutagenesis in human
851 mitochondrial DNA. *J. Mol. Biol*, **273**(2), 417–427.
852 https://doi.org/10.1006/jmbi.1997.1268 (1997).
853 43. Furtado, C. *et al*. Functional characterization of 8-oxoguanine DNA glycosylase of
854 Trypanosoma cruzi. *PloS one*, **7**(8), e42484.
855 https://doi.org/10.1371/journal.pone.0042484 (2012).
856 44. Kunrath-Lima, M. *et al*. Characterization of Trypanosoma cruzi MutY DNA
857 glycosylase ortholog and its role in oxidative stress response. *Infect. Genet. Evol.*
858 55, 332–342 https://doi.org/10.1016/j.meegid.2017.09.030 (2017).
859 45. Aguiar, P. H. N. *et al*. Oxidative stress and DNA lesions: the role of 8-oxoguanine
860 lesions in Trypanosoma cruzi cell viability. *PLoS Negl. Trop. Dis*, **7**(6), e2279.
861 https://doi.org/10.1371/journal.pntd.0002279 (2013).
862 46. Lopes, D. de O. *et al*. Biochemical studies with DNA polymerase β and DNA
863 polymerase β-PAK of Trypanosoma cruzi suggest the involvement of these proteins
864 in mitochondrial DNA maintenance. *DNA Repair (Amst)*, **7**(11), 1882–1892.
865 https://doi.org/10.1016/j.dnarep.2008.07.018 (2008).
866 47. Schamber-Reis, B. L. F. *et al*. DNA polymerase beta from Trypanosoma cruzi is
867 involved in kinetoplast DNA replication and repair of oxidative lesions. *Mol.*
868 *Biochem. Parasitol*. **183**(2), 122–131.
869 https://doi.org/10.1016/j.molbiopara.2012.02.007 (2012).
870 48. Rajão, M. A. *et al*. DNA polymerase kappa from Trypanosoma cruzi localizes to the
871 mitochondria, bypasses 8-oxoguanine lesions and performs DNA synthesis in a
872 recombination intermediate. *Mol. Microbiol.* **71**(1), 185–197.
873 https://doi.org/10.1111/j.1365-2958.2008.06521.x (2009).

874 49. Vieira-da-Rocha, J. P. *et al*. The DNA damage response is developmentally
875 regulated in the African trypanosome. *DNA Repair* (Amst). **73**, 78–90
876 https://doi.org/10.1016/j.dnarep.2018.11.005 (2018).
877 50. Warren L. G. Metabolism of *Schizotrypanum cruzi* Chagas. I. Effect of culture age
878 and substrate concentration on respiratory rate. *The Journal of parasitology*, **46**,
879 529–539 (1960).
880 51. Beneke, T. *et al.* A CRISPR Cas9 high-throughput genome editing toolkit for
881 kinetoplastids. *Royal Society open science*, **4**(5), 170095.
882 https://doi.org/10.1098/rsos.170095 (2017).
883 52. Peng, D., & Tarleton, R. EuPaGDT: a web tool tailored to design CRISPR guide
884 RNAs for eukaryotic pathogens. *Microbial genomics*, ***1***(4), e000033.
885 https://doi.org/10.1099/mgen.0.000033 (2015).
886 53. Davey, J. W. *et al.* Chromosomal assembly of the nuclear genome of the
887 endosymbiont-bearing trypanosomatid Angomonas deanei. *G3 (Bethesda,*
888 *Md.)*, **11**(1), jkaa018. https://doi.org/10.1093/g3journal/jkaa018 (2021).
889 54. Andrade, I. d. S., *et al.* Characterization of a porin channel in the endosymbiont of
890 the trypanosomatid protozoan Crithidia deanei. *Microbiology,* **157***(10), 2818–*
891 *2830.* https://doi.org/10.1099/mic.0.049247-0 (2011)
892 55. Liu, Y., & Englund, P. T. The rotational dynamics of kinetoplast DNA replication.
893 *Mol. Microbiol.,* **64***(3), 676–690.* doi:10.1111/j.1365-2958.2007.05686.x (2007).
894 56. Santos, J.H., Meyer,J.N., Mandavilli,B.S. and Van Houten,B. Quantitative PCR-
895 based measurement of nuclear and mitochondrial DNA damage and repair in
896 mammalian cells. *Methods Mol. Biol.* 7:183. https://doi:10.1385/1-59259-973-7:183
897 (2006).
898 57. Huang, H., Zhu, L., Reid, B. R., Drobny, G. P., & Hopkins, P. B. Solution structure
899 of a cisplatin-induced DNA interstrand cross-link. *Science* **270** (5243), 1842–1845.
900 https://doi.org/10.1126/science.270.5243.1842 (1995).
901 58. Ohndorf, U. M., Rould, M. A., He, Q., Pabo, C. O., & Lippard, S. J. Basis for
902 recognition of cisplatin-modified DNA by high-mobility-group
903 proteins. *Nature*, **399** (6737), 708–712. https://doi.org/10.1038/21460 (1999).
904 59. Siddik, Z. H. Cisplatin: Mode of cytotoxic action and molecular basis of resistance.
905 *Oncogene* **22** 7265–7279. https://doi:10.1038/sj.onc.1206933 (2003).

60. Alt, A. *et al.* Bypass of DNA lesions generated during anticancer treatment with cisplatin by DNA polymerase eta. *Science*, **318**(5852), 967–970. https://doi.org/10.1126/science.1148242 (2007).
61. Todd, R. C., & Lippard, S. J. Inhibition of transcription by platinum antitumor compounds. *Metallomics : integrated biometal science*, **1**(4), 280–291. https://doi.org/10.1039/b907567d (2009).
62. Morales, J., *et al.* Development of a toolbox to dissect host-endosymbiont interactions and protein trafficking in the trypanosomatid Angomonas deanei. *BMC Evol Biol*, **16**(1), 247. https://doi.org/10.1186/s12862-016-0820-z (2016).
63. Beneke, T., *et al.* Genetic dissection of a Leishmania flagellar proteome demonstrates requirement for directional motility in sand fly infections. *PLoS pathogens*, **15**(6), e1007828. https://doi.org/10.1371/journal.ppat.1007828 (2019)
64. Soares Medeiros, L. C. *et al*. Rapid, Selection-Free, High-Efficiency Genome Editing in Protozoan Parasites Using CRISPR-Cas9 Ribonucleoproteins. *mBio*, **8**(6), e01788-17. https://doi.org/10.1128/mBio.01788-17 (2017).
65. Beck, K. *et al*. *Trypanosoma brucei* Tb927.2.6100 is an essential protein associated with kinetoplast DNA. *Eukaryotic cell*, **12**(7), 970–978. https://doi.org/10.1128/EC.00352-12 (2013).
66. Hammarton T. C. Cell cycle regulation in *Trypanosoma brucei*. *Mol Biochem Parasitol*, **153**(1), 1–8. https://doi.org/10.1016/j.molbiopara.2007.01.017 (2007).
67. Jones, N. G. *et al.* Regulators of *Trypanosoma brucei* cell cycle progression and differentiation identified using a kinome-wide RNAi screen. *PLoS pathogens*, **10**(1), e1003886. https://doi.org/10.1371/journal.ppat.1003886 (2014).
68. Pasternack, D. A., *et al.* Sphingosine Kinase Regulates Microtubule Dynamics and Organelle Positioning Necessary for Proper G1/S Cell Cycle Transition in *Trypanosoma brucei*. *mBio*, **6**(5), e01291-15. https://doi.org/10.1128/mBio.01291-15 (2015).
69. Benz, C., & Urbaniak, M. D. Organising the cell cycle in the absence of transcriptional control: Dynamic phosphorylation co-ordinates the *Trypanosoma brucei* cell cycle post-transcriptionally. *PLoS pathogens*, **15**(12), e1008129. https://doi.org/10.1371/journal.ppat.1008129 (2019).

70. Klebanov-Akopyan, O. *et al. Trypanosoma brucei* UMSBP2 is a single-stranded telomeric DNA binding protein essential for chromosome end protection. *Nucleic acids research*, **46**(15), 7757–7771. https://doi.org/10.1093/nar/gky597 (2018).
71. Li, Y., Sun, Y., Hines, J. C., & Ray, D. S. Identification of new kinetoplast DNA replication proteins in trypanosomatids based on predicted S-phase expression and mitochondrial targeting. *Eukaryotic cell*, **6**(12), 2303–2310. https://doi.org/10.1128/EC.00284-07 (2007).
72. Amodeo, S., Jakob, M., & Ochsenreiter, T. Characterization of the novel mitochondrial genome replication factor MiRF172 in *Trypanosoma brucei*. *Journal of cell science*, **131**(8), jcs211730. https://doi.org/10.1242/jcs.211730 (2018).
73. Týč, J., Klingbeil, M. M., & Lukeš, J. Mitochondrial heat shock protein machinery hsp70/hsp40 is indispensable for proper mitochondrial DNA maintenance and replication. *mBio*, **6**(1), e02425-14. https://doi.org/10.1128/mBio.02425-14 (2015).
74. Brueckner, F., Hennecke, U., Carell, T., & Cramer, P. CPD damage recognition by transcribing RNA polymerase II. *Science*, **315**(5813), 859–862. https://doi.org/10.1126/science.1135400 (2007).
75. Hanawalt, P. C., & Spivak, G. Transcription-coupled DNA repair: two decades of progress and surprises. *Nature reviews. Molecular cell biology*, **9**(12), 958–970. https://doi.org/10.1038/nrm2549 (2008).
76. McCulloch, R., & Barry, J. D. A role for RAD51 and homologous recombination in *Trypanosoma brucei* antigenic variation. *Genes & development*, **13**(21), 2875–2888. https://doi.org/10.1101/gad.13.21.2875 (1999).
77. Dobson, R. *et al.* Interactions among *Trypanosoma brucei* RAD51 paralogues in DNA repair and antigenic variation. *Molecular microbiology*, **81**(2), 434–456. https://doi.org/10.1111/j.1365-2958.2011.07703.x (2011).
78. Grazielle-Silva, V. *et al. Trypanosoma brucei* and *Trypanosoma cruzi* DNA Mismatch Repair Proteins Act Differently in the Response to DNA Damage Caused by Oxidative Stress. *Front Cell Infect Microbiol*, **10**, 154. https://doi.org/10.3389/fcimb.2020.00154 (2020).

Acknowledgement

This work was supported by CNPq and FAPERJ. JCM is supported by the Wellcome Trust (200807/Z/16/Z).

Author Contributions

Conceived and designed the experiments: MCMM CRM CMCC-P. Acquisition of data: CSG CMCC-P BR Analyzed the data: MCMM CRM CSG CMCC-P BR JCM WS Contributed reagents/materials: MCMM CRM JCM WS. Wrote the paper: MCMM CRM CMCC-P CSG BR. Revised the paper: CSG CMCC-P BR WS JCM CRM MCMM

Figure Legends

Figure 1: Generation of *KAP4* mutants, cell proliferation and viability. qPCR amplification showing that there was no damage to the nuclear (**a**) and mitochondrial (**b**) DNA of the T7RNAPol-SpCas9 cells compared to WT cells. (**c**) Diagram representing the sgRNA PCR transfection that allows for double strain breaks (DSBs) at the 5' and 3' ends of the genes and repair-templates mediated recombination at the UTRs 30 nt upstream and downstream of the CDS. Diagnostic PCR oligonucleotides were designed to amplify the integrated NEO repair template, binding upstream of the open reading frame (OL5) and internally to the NEO gene (OL6), and the presence (WT and +/-) or absence (-/-) of *KAP4* (650 bp, OL5+OL7). (**d**) Diagnostic PCR showing *KAP4* gene deletion and Neo selectable marker integration in the *A. deanei* genome. (**e**) Growth curve for 72 h showed that *KAP4* mutants present a reduced proliferation in relation to WT and T7RNAPol-SpCas9 strains. Cell number was plotted on a logarithmic scale, and the presented data are the mean ± s.d. of three independent cell cultures. After 48 h, when cells reached the peak of the exponential phase, a paired T test ($p<0.05$) was performed to compare control and mutant cells. (**f**) Duplication time of WT, T7RNAPol-SpCas9 and cells deleted for *KAP4*. (**g**) The cell viability was similar among the strains analyzed and maintained even after 72 h of cultivation. The presented data is a mean ± s.d. of three independent cell cultures. WT, wild-type cells, $kap4^{+/-}$, cells with deletion for one allele, $kap4^{-/-}$, null mutant.

Figure 2: Ultrastructure and morphology of *A. deanei*. WT (**a-c**), T7RNAPol-SpCas9 (**d-f**) and *KAP4* mutant cells with single (**g-l**) or double deletions (**m-r**). (**a-b**) Transmission

electron microscopy of WT cells showed typical characteristics of symbiont-harboring trypanosomatids, which were also observed in T7RNAPol-SpCas9 cells (**d-e**). *kap4*$^{+/-}$ and *kap4*$^{-/-}$ cells presented ultrastructural alterations as a high condensation of nuclear DNA (**g**), a densely packed kDNA (**i-o**), a filamentous symbiont (**h**, **n**), dividing cells with two flagella in the same flagellar pocket (**m**). Scanning electron microscopy showed the typical choanomastigote form in WT and T7RNAPol-SpCas9 cells of mutant cells (**c** and **f**). *kap4*$^{+/-}$ mutants presented ultrastructure alterations such as asymmetric division (**j**, yellow arrow), which generated cells with different dimensions (**k**) and protozoa with multiple cell bodies and flagella (**l**). *kap4*$^{-/-}$ cells presented cytokinesis impairment that generated a popcorn-like phenotype (**q-r**). In both mutant strains, cell bodies and flagellum shortening were observed (**j** and **p**, white arrows). ht – heterochromatin, k-kinetoplast, lb - lipid body, n - nucleus, nu - nucleolus, s - symbiont, f – flagellum, fs - filamentous symbiont, v - vacuole. Brackets show the more densely packed kDNA.

Figure 3: Atypical phenotypes were observed in *KAP4* mutant cells cultivated for 24 h after labeling with DAPI and anti-porin antibodies. WT (**a-a"**); *kap4*$^{+/-}$ mutants containing one filamentous symbiont with multiple nucleoids (Fs - green arrowhead), one nucleus (N-white arrows) and one kinetoplast (K-white arrowhead) (**b-b"**) or two nuclei and two kinetoplasts and (**c-c"**); *kap4*$^{-/-}$ cells were seen with one filamentous symbiont, two nuclei and one kinetoplast (**d-d"**). Bars 5 μm. (**e**) Counting of cellular patterns showing that filamentous symbionts (Fs) are more frequent in *kap4*$^{-/-}$. (**f**) Percentage of cells presenting atypical phenotypes. (g) *In situ* labeling showing the different stages of kDNA network replication in WT and mutant cells (according to Liu and Englund 2007)[15]. Green arrowheads indicate the symbiont, white arrows the nucleus and white arrowheads the kinetoplast. Bars 1 μm. t test p-value < 0.005. A total of 1,000 WT and KAP4 mutant cells were counted in 3 independent experiments.

Figure 4: Cell growth and survival after cisplatin treatment or UV radiation. After 12 h, no remarkable differences were observed in cell proliferation and survival when comparing WT and mutant protozoa after treatment with 150 μM and 300 μM cisplatin (**a-b**) or exposure to UV radiation (**c-d**).

Figure 5: Effects of cisplatin on the ultrastructure of mutant cells as revealed by TEM (**a-c**, **f-h**, **k-m**) and SEM (**d-e**, **i-j**, **n-o**). A-E: WT cells treated with cisplatin did not present ultrastructural alterations by TEM. However, SEM showed rounded cells with a shortening flagellum (**d-e**). (**f-o**) mutant cells treated with cisplatin. (**f**) Note DNA unpacking in the nucleus (n), the proximity between the ER (black arrowhead) and the endosymbiont, and mitochondrial branch swelling (m). (**g**, **l**) The symbiotic bacterium presents alterations in the nuclear matrix and DNA condensation (white arrows). (**k**-**l**): The symbiont presented membrane convolutions (black arrow) and was surrounded by vacuoles, an indication of autophagy. (**h**, **m**) In mutant cells, the kDNA arrangement was not affected in relation to protozoa not submitted to cisplatin treatment. n - nucleus, k - kinetoplast, m - mitochondrial branch, s - symbiont, v - vacuole. (**d**-**e**, **i**-**j**, **n**-**o**) WT and mutant cells of both types treated with cisplatin presented a rounded format containing a shortening flagellum. Other atypical phenotypes, such as fat-cell shape (**d**), lack of flagellum (**i** and **n,** arrowheads) and plasma membrane blebs (**o**, arrows), were also observed.

Figure 6: DAPI-stained mutant protozoa presented different atypical phenotypes when compared to WT cells after treatment with cisplatin for over 24 h (**a**-**c**). (**a-a**") WT cells treated with 150 µM cisplatin presented rounded shapes, and the fat cell phenotype contained a symbiont with multiple nucleoids (white square, green arrowheads). (**b-b"**) Ad kap4$^{(+/-)}$ cells treated with 300 µM cisplatin lacking the symbiont. (**c-c"**) Ad kap4$^{(-/-)}$ cells treated with 300 µM cisplatin containing one filamentous symbiont, two nuclei and one kinetoplast. (**d)** Counting of cellular patterns considering the presence of normal or filamentous symbionts. (**e**) Percentage of cells with atypical phenotypes. Bars 5 µm. Fs - Filamentous symbiont.; N- nucleus - white arrows; K-kinetoplast - white arrowheads. A total of 1,000 cells of WT and KAP4 mutant cells were counted in 3 independent experiments.

Figure 7: Effects of UV irradiation on the ultrastructure of WT and mutant cells as revealed by TEM (**a-b, f-g, k-l**) and SEM (**c-e, h-j, m-o**). (**a-b)** WT cells submitted to irradiation. Nuclear DNA condensation and kDNA arrangement were not modified. However, the symbiont genome became densely packed (**a**, arrows). (**f-g, k-l**) mutant

cells submitted to UV irradiation. Nuclear DNA condensation and kDNA arrangement were not affected. (**f, k, g**) The symbiont was seen in association with the ER (white arrowheads), and its DNA suffered condensation (white arrows). (**l**) *kap4*$^{-/-}$ cells containing multiple nuclei were also observed. fp - flagellar pocket, g - glycosome, k - kinetoplast, m - mitochondrion, n - nucleus, s - symbiont. (**a-c**) WT cells subjected to irradiation presented atypical formats indicating cytokinesis impairment. (**h-j**) *kap4*$^{+/-}$ cells submitted to UV irradiation presented multiple interconnected cell bodies, indicating that in such mutants, cytokinesis impairment was exacerbated in relation to WT protozoa. (**m-o**) *kap4*$^{-/-}$ cells submitted to UV irradiation presented a round cell body, and the flagellum was short or even absent (white arrows).

Figure 8: DAPI-stained protozoa exposed to UV irradiation presented atypical phenotypes. Such morphotypes were observed in WT cells (**a-a"**), as well as in kap4$^{+/-}$ (**b-b"**) and kap4$^{-/-}$ (**c-c''**) mutant cells. (**a-a"**) Protozoa harboring two symbionts, two nuclei, and one kinetoplast. (**b-b"**) A dyskinetoplastic protozoan, with a filamentous symbiont containing multiple nucleoids and one nucleus. (**c-c''**) A cured cell containing one nucleus and one kinetoplast. (**d**) Counting of cellular patterns considering the presence of normal or filamentous symbionts, as well as cured cells (that lost the symbiont) or lysed symbionts. (**e**) Percentage of cells presenting atypical phenotypes. S-Symbiont and Fs - Filamentous symbiont, green arrowheads indicate bacterium nucleoids; N- nucleus - white arrows; K-kinetoplast - white arrowhead. Bars 5 µm. A total of 1,000 WT and KAP4 mutant cells were counted in 3 independent experiments.

Figure 9: DNA repair kinetics of WT and mutant cells. (**a-b**) DNA repair kinetics of WT cells compared to *kap4*$^{+\backslash-}$ cells (left panel) and *kap4*$^{-\backslash-}$ (right panel) after treatment with 300 µM cisplatin. (**c-d**) DNA repair kinetics of WT cells in relation to *kap4*$^{+\backslash-}$ cells (left panel) and *kap4*$^{-\backslash-}$ (right panel) after UV damage radiation. As observed for cisplatin, no significant difference was observed in the DNA repair kinetics of all cell types.

Table 1: List of oligonucleotides for CRISPR-Cas9 in *A. deanei*, including sgRNA, repair template and diagnostic PCR. Sequences are written in the 5' to 3' orientation.

Supplementary Material 1: Total protein extract of WT and T7RNAPol-SpCas9 mutant strains of *A. deanei* and *L. mexicana*, here used as a control, were probed with anti-FLAG antibody (Anti-FLAG M2, Sigma F3165; dilution 1:20,000) for detection of SpCas9 or anti-β-tubulin (Anti-β-Tubulin clone AA2, Sigma T8328; dilution 1:10,000) used as loading control.

Supplementary Material 2: Flow cytometry analysis of *A. deanei* DNA content in wild type (WT) and mutant cells treated or not with cisplatin for 1 h or 24 h.

Supplementary Material 3: DNA repair kinetics (0.25-6 h) measured by long-range qPCR. Absorbance values for the smaller fragments of *A. deanei* WT, *kap4*$^{+/-}$ and *kap4*$^{-/-}$.

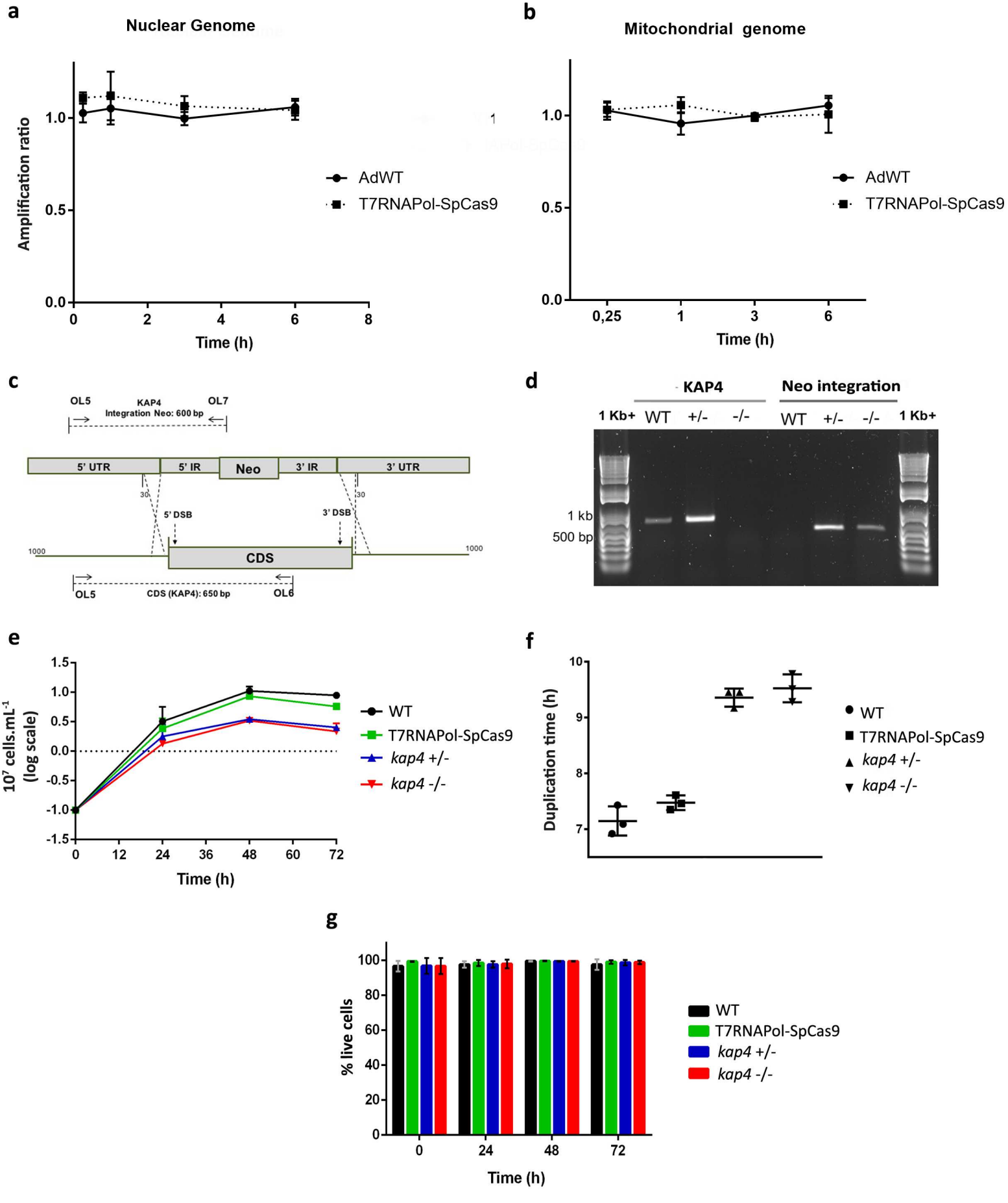
a
Nuclear Genome
Amplification ratio
1.0
0.5
0.0
0
2
4
6
8
Time (h)
AdWT
T7RNAPol-SpCas9
b
Mitochondrial genome
1.0
0.5
0.0
0,25
1
3
6
Time (h)
AdWT
T7RNAPol-SpCas9
c
OL5
KAP4
Integration Neo: 600 bp
OL7
5' UTR
5' IR
Neo
3' IR
3' UTR
30
30
5' DSB
3' DSB
1000
1000
CDS
OL5
CDS (KAP4): 650 bp
OL6
d
KAP4
Neo integration
1 Kb+
WT
+/-
-/-
WT
+/-
-/-
1 Kb+
1 kb
500 bp
e
10⁷ cells.mL⁻¹
(log scale)
1.5
1.0
0.5
0.0
-0.5
-1.0
-1.5
0
12
24
36
48
60
72
Time (h)
WT
T7RNAPol-SpCas9
kap4 +/-
kap4 -/-
f
Duplication time (h)
10
9
8
7
WT
T7RNAPol-SpCas9
kap4 +/-
kap4 -/-
g
% live cells
100
80
60
40
20
0
0
24
48
72
Time (h)
WT
T7RNAPol-SpCas9
kap4 +/-
kap4 -/-

WT
T7RNAPol-SpCas9
kap4 +/-
kap4 -/-
a
b
c
d
e
f
g
h
i
j
k
l
m
n
o
p
q
r
nu
ht
s
k
fs
lb
LB
v
500 nm
200 nm
2 µm
1 µm
4 µm

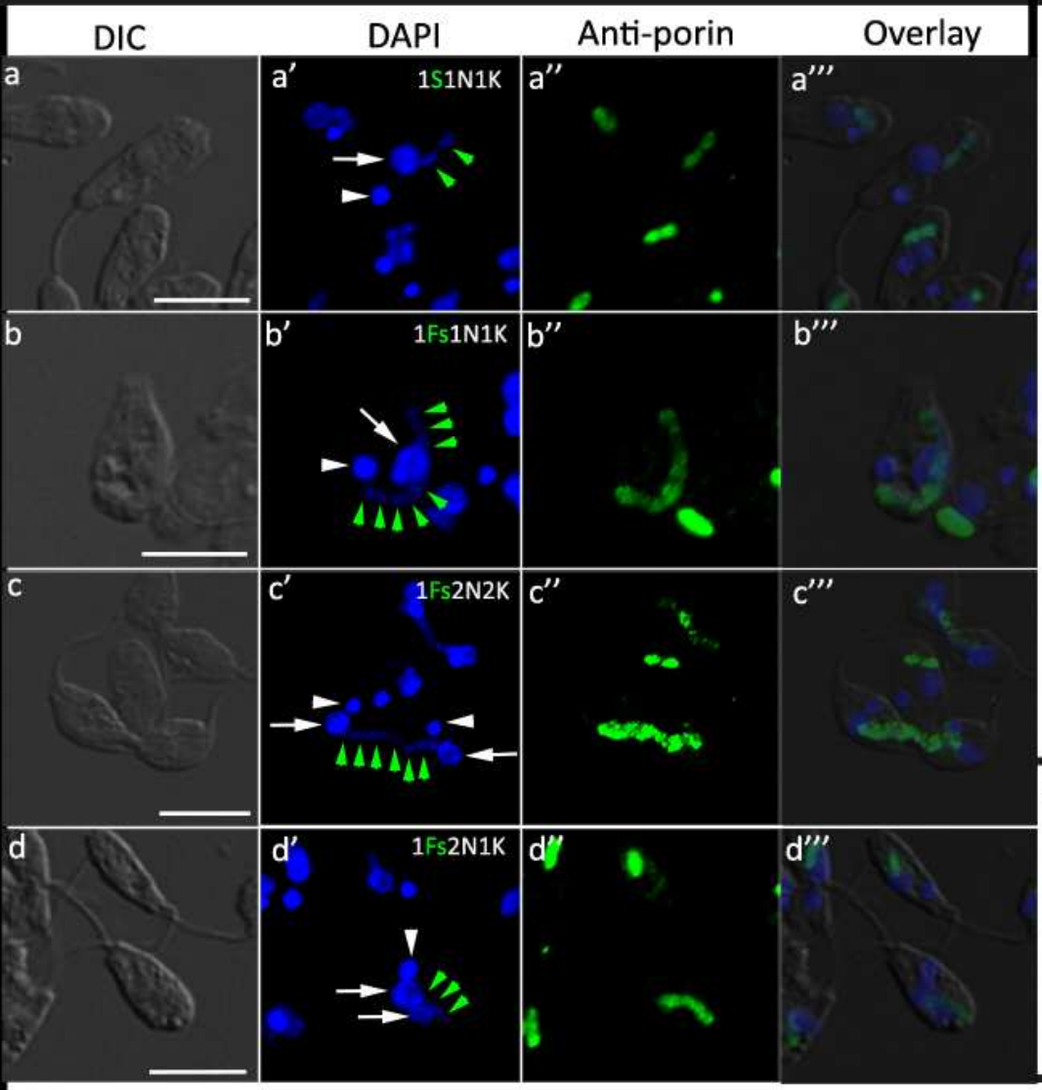

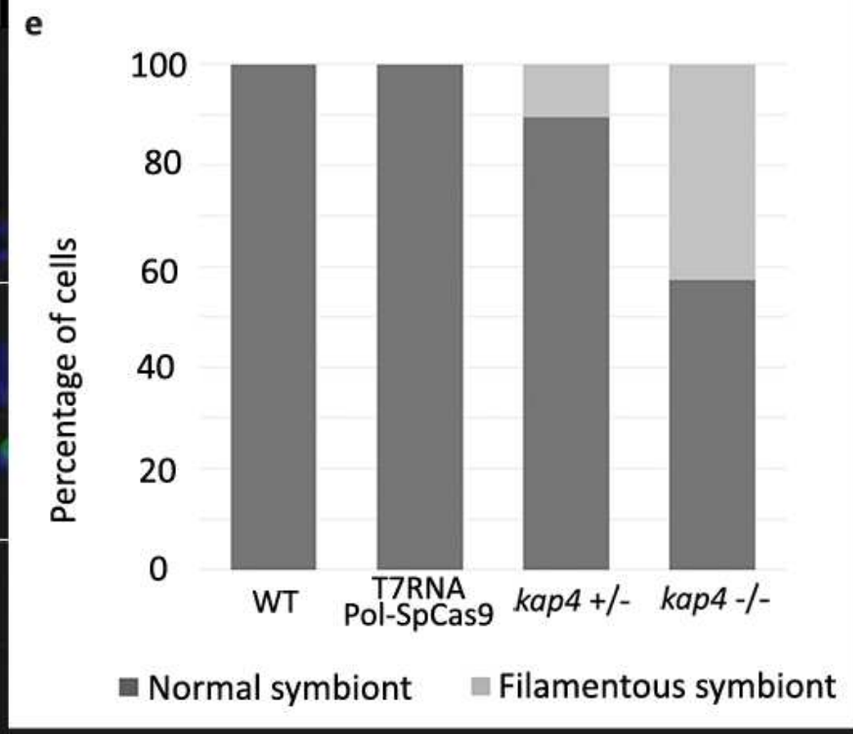

f

Atypical phenotypes	WT	T7RNAPol-SpCas9	*kap4 +/-*	*kap4 -/-*
1Fs1N1K	0,0%	0,0%	9,0%	39,3%
1Fs1N2K	0,0%	0,0%	0,0%	1,1%
1Fs2N2K	0,0%	0,0%	0,8%	0,0%
1Fs2N1K	0,0%	0,0%	0,8%	2,2%

g

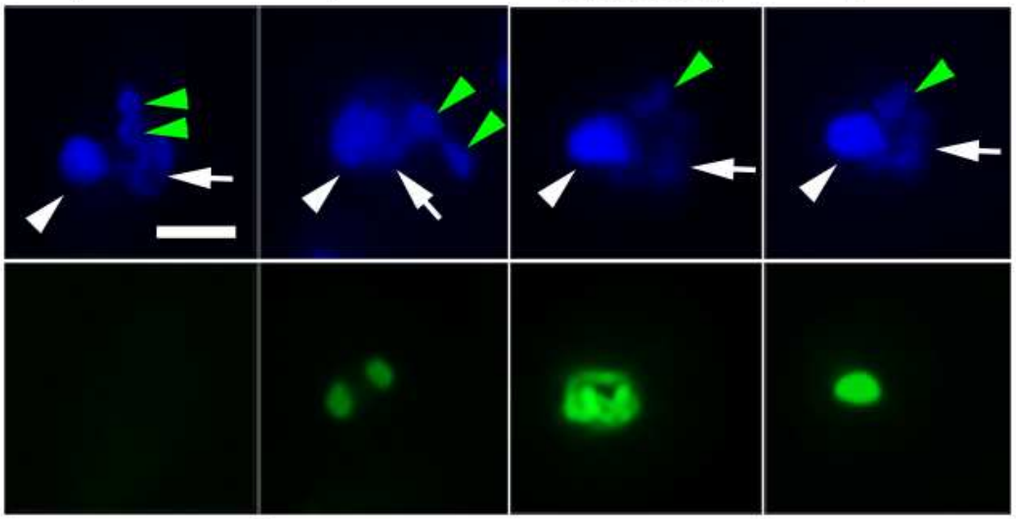

WT	76%	8%	5%	11%
kap4 +/-	74%	6%	5%	15%
kap4 -/-	80%	3%	6%	11%

Cisplatin treatment

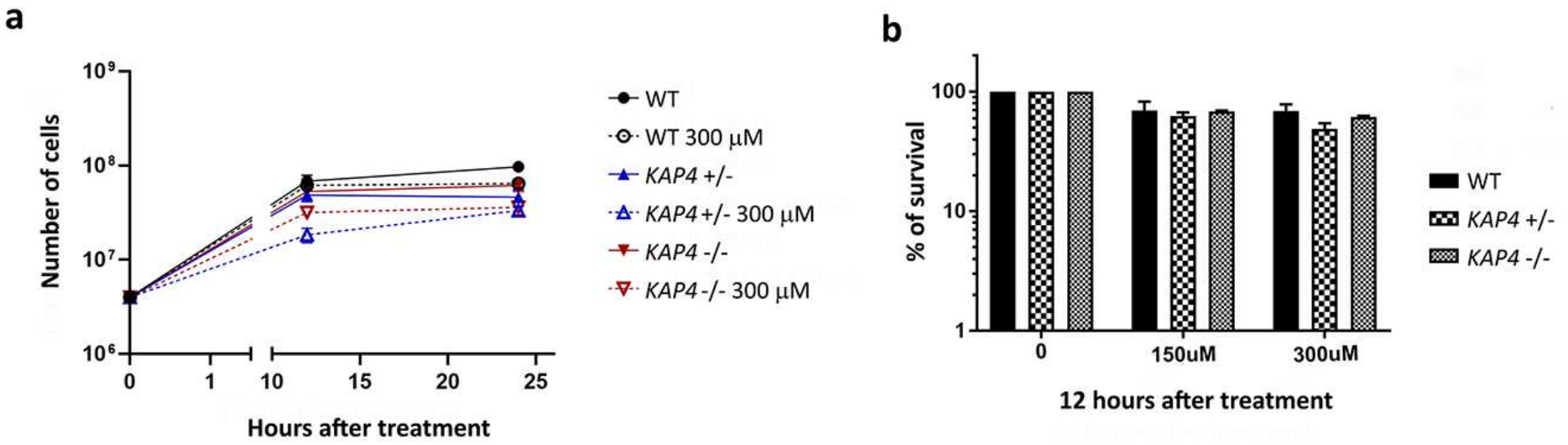

Ultraviolet radiation

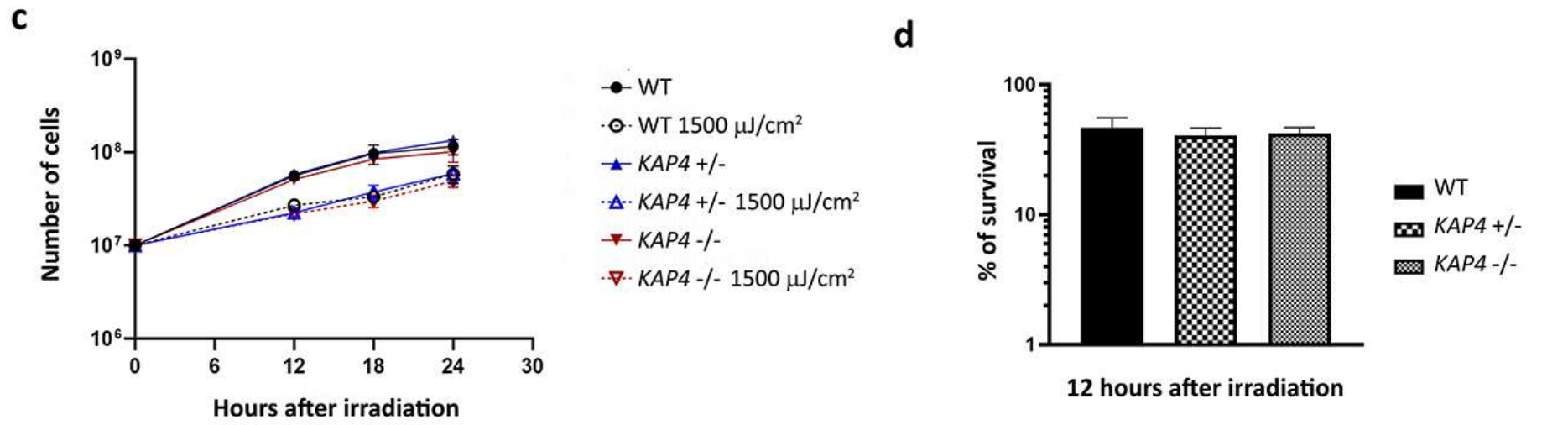

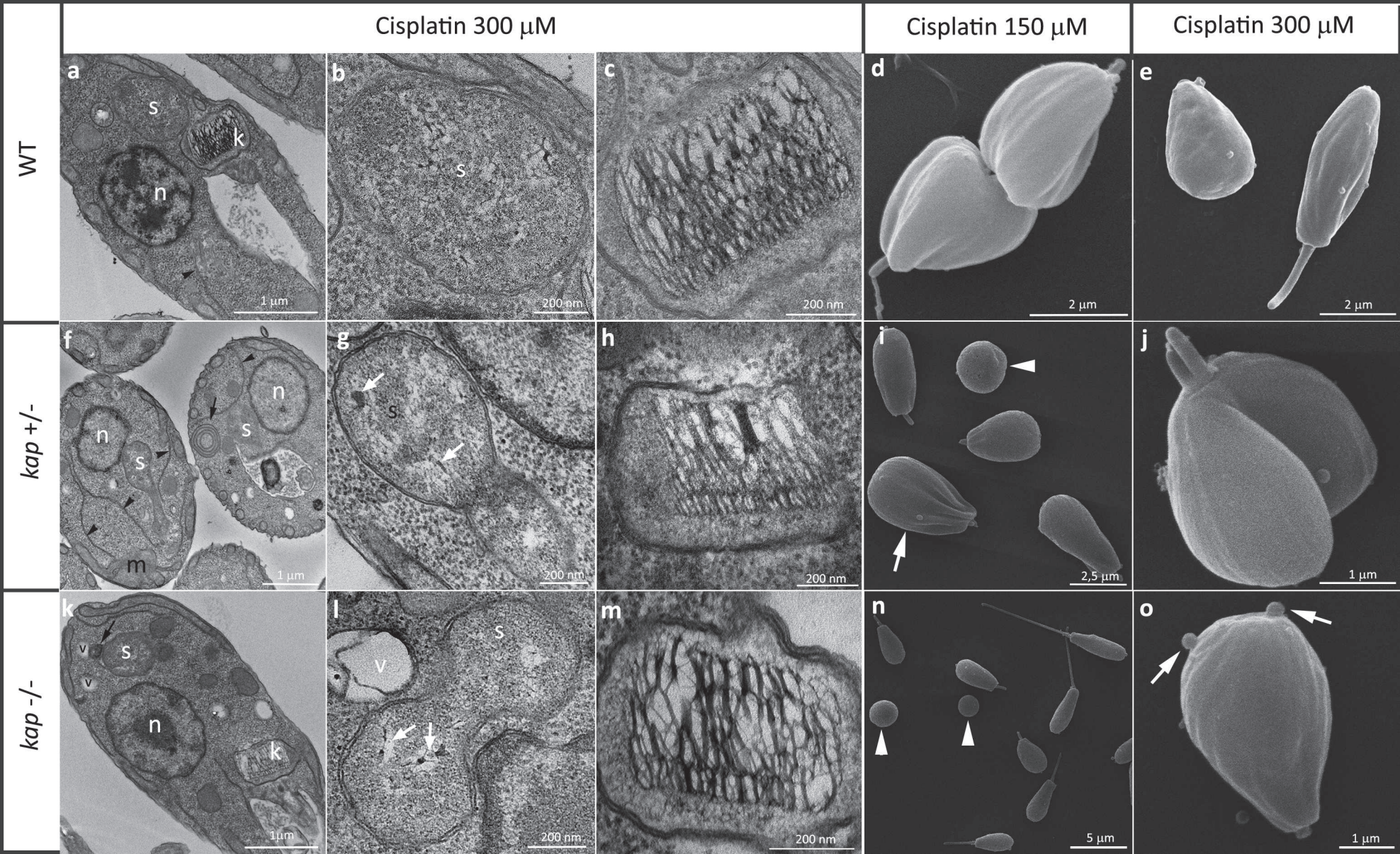
Cisplatin 300 μM
Cisplatin 150 μM
Cisplatin 300 μM
WT
kap +/-
kap -/-
a
b
c
d
e
f
g
h
i
j
k
l
m
n
o
s
k
n
m
v
1 μm
200 nm
2 μm
2,5 μm
5 μm

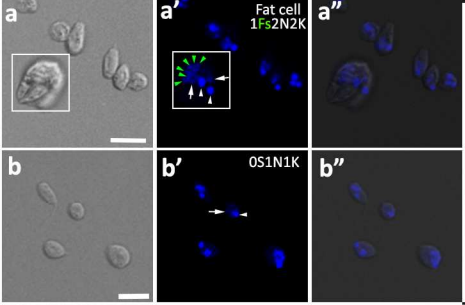

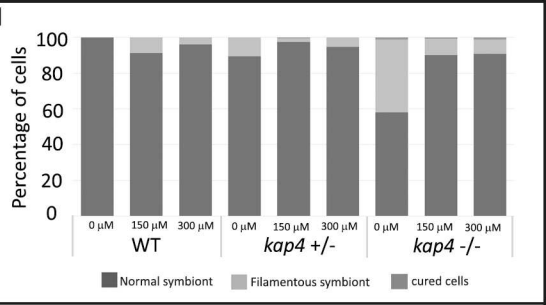

e

Atypical phenotypes	WT			*kap4 +/-*			*kap4 -/-*		
	0 µM	150 µM	300 µM	0 µM	150 µM	300 µM	0 µM	150 µM	300 µM
1Fs1N1K	0,0%	7,8%	4,0%	9,0%	1,9%	5,3%	39,8%	9,2%	7,7%
1Fs2N2K	0,0%	1,0%	0,0%	0,8%	0,0%	0,0%	0,0%	0,0%	0,0%
1Fs2N1K	0,0%	0,0%	0,0%	0,8%	0,0%	0,0%	1,1%	0,0%	0,4%
0S1N1K	0,0%	0,0%	0,0%	0,0%	0,6%	0,0%	1,1%	0,8%	1,2%

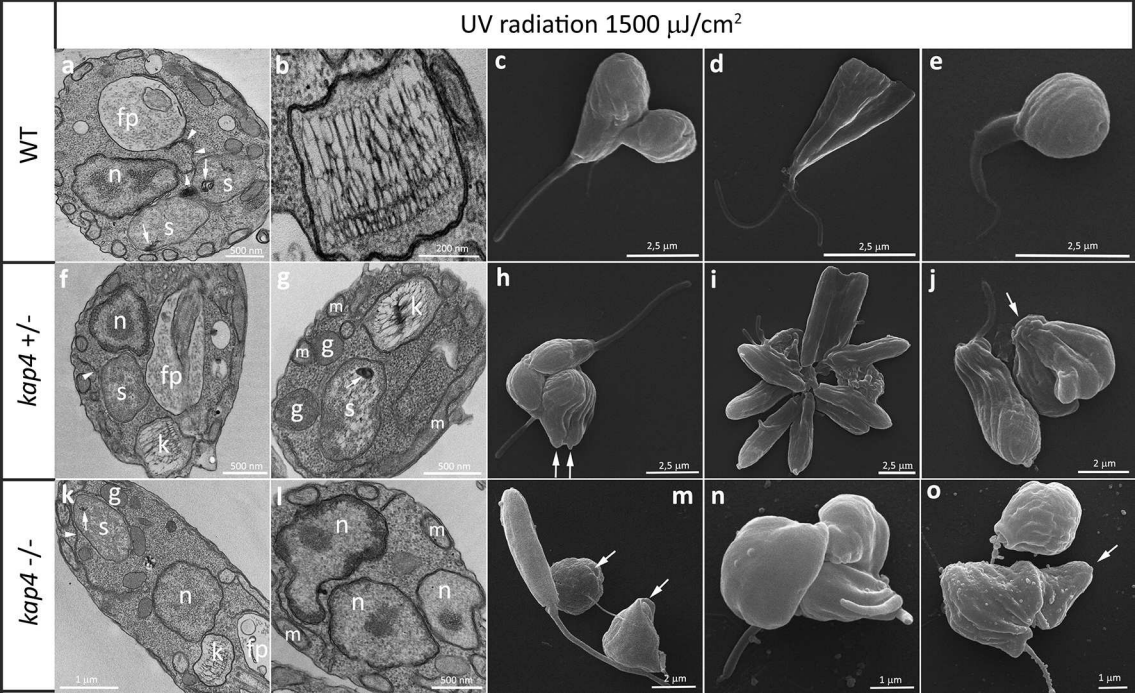
UV radiation 1500 μJ/cm²
WT
kap4 +/-
kap4 -/-
a
b
c
d
e
f
g
h
i
j
k
l
m
n
o
fp
n
s
k
m
g
500 nm
200 nm
2,5 μm
2 μm
1 μm

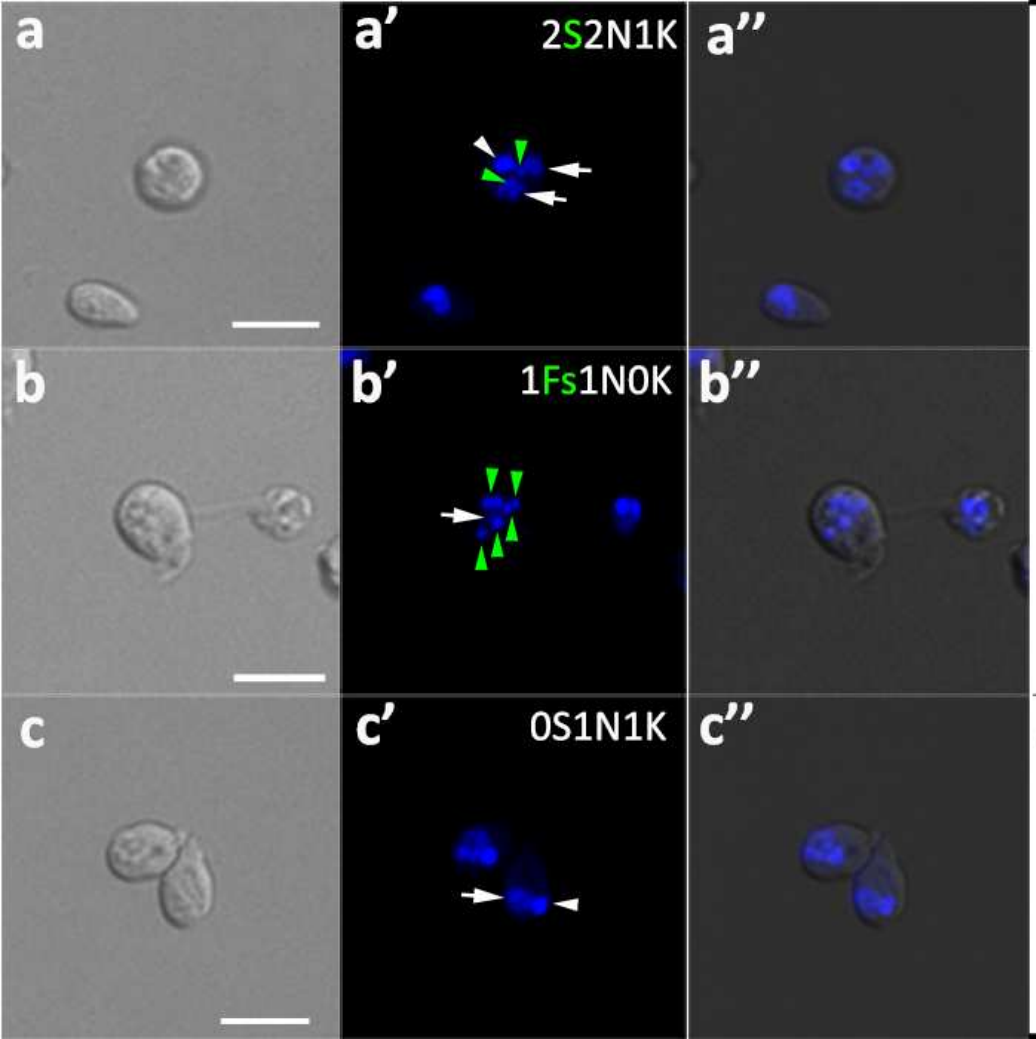

d

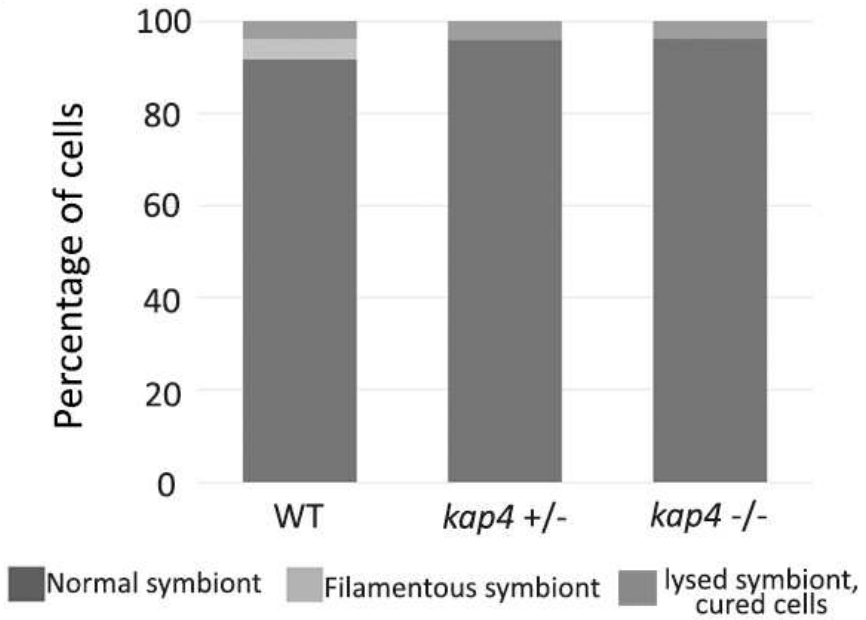

e

Atypical phenotypes	WT	*kap4 +/-*	*kap4 -/-*
2S2N1K	1,5%	0,0%	1,6%
1S2N1K	0,0%	1,7%	3,1%
1S2N0K	0,0%	0,0%	0,8%
1Fs1N1K	3,7%	0,0%	0,0%
1Fs1N0K	0,7%	0,0%	0,0%
0S1N1K	0,7%	2,9%	2,3%
Fragmented DNA	3,0%	1,1%	1,6%

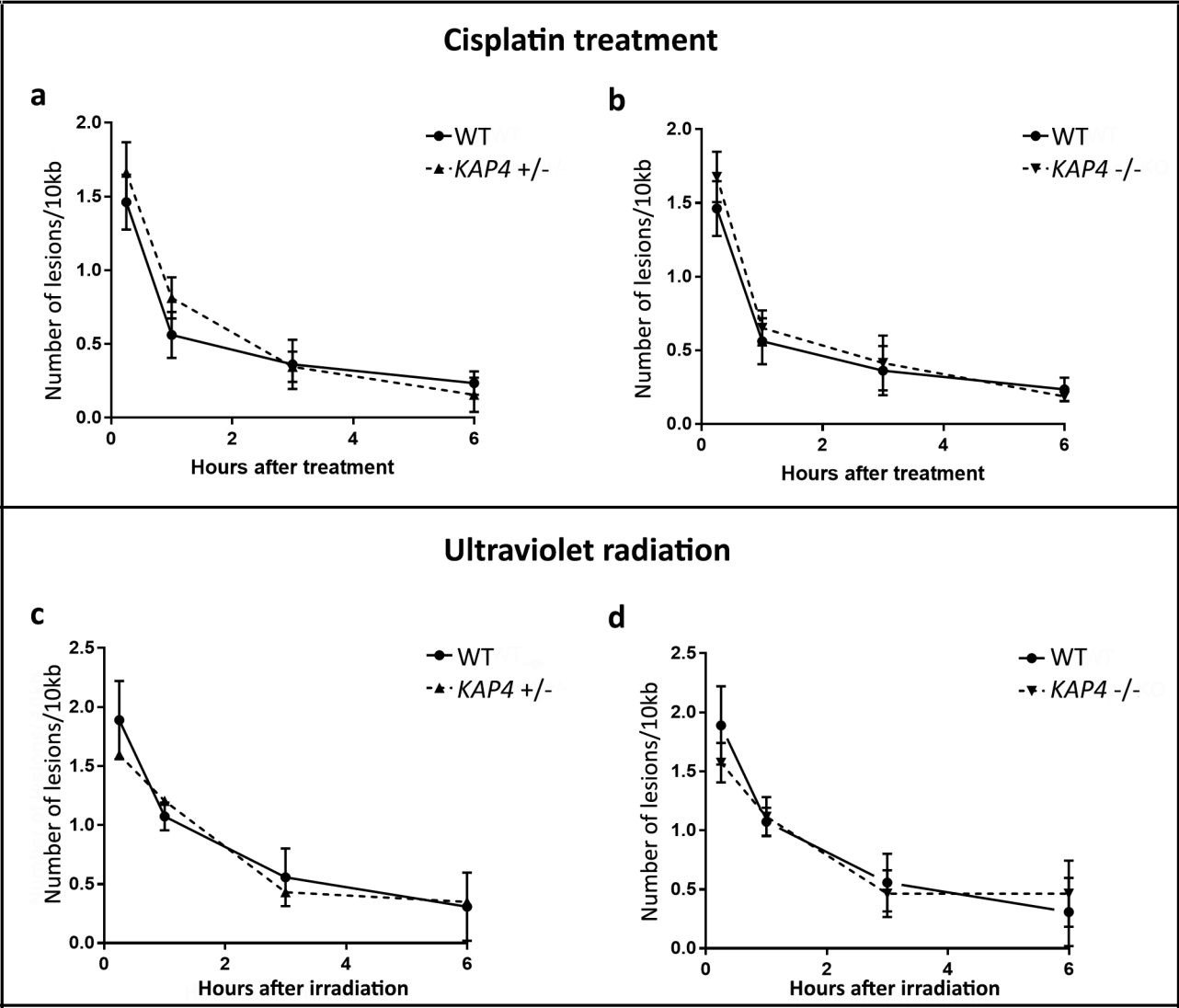
Cisplatin treatment
a
b
WT
KAP4 +/-
KAP4 -/-
Number of lesions/10kb
Hours after treatment
Ultraviolet radiation
c
d
Hours after irradiation

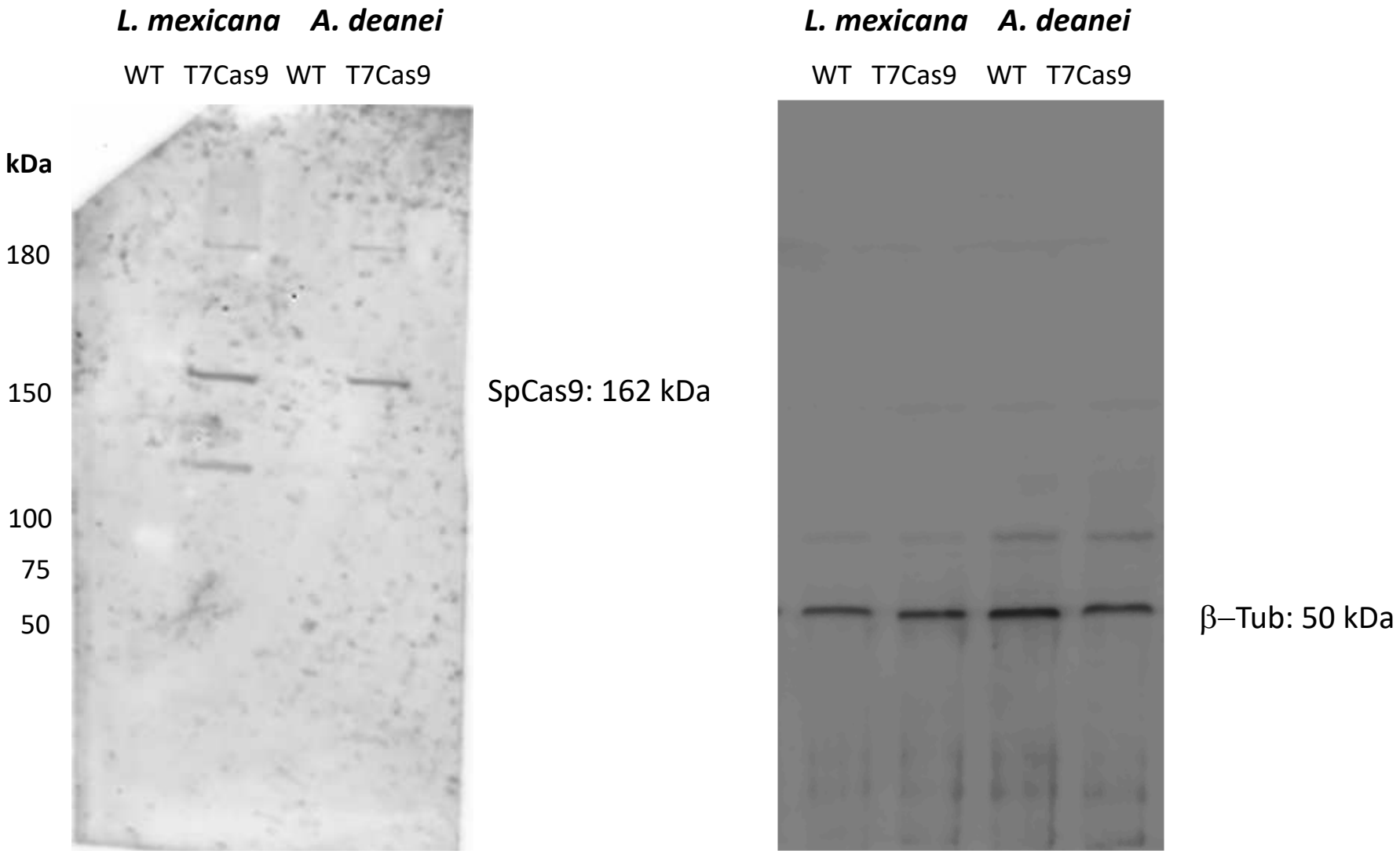

Supplementary Material 1: Total protein extract of WT and T7RNAPol-SpCas9 mutant strains of *A. deanei* and *L. mexicana*, here used as a control, were probed with anti-FLAG antibody (Anti-FLAG M2, Sigma F3165; dilution 1:20,000) for detection of SpCas9 or anti-β-tubulin (Anti-β-Tubulin clone AA2, Sigma T8328; dilution 1:10,000) used as loading control.

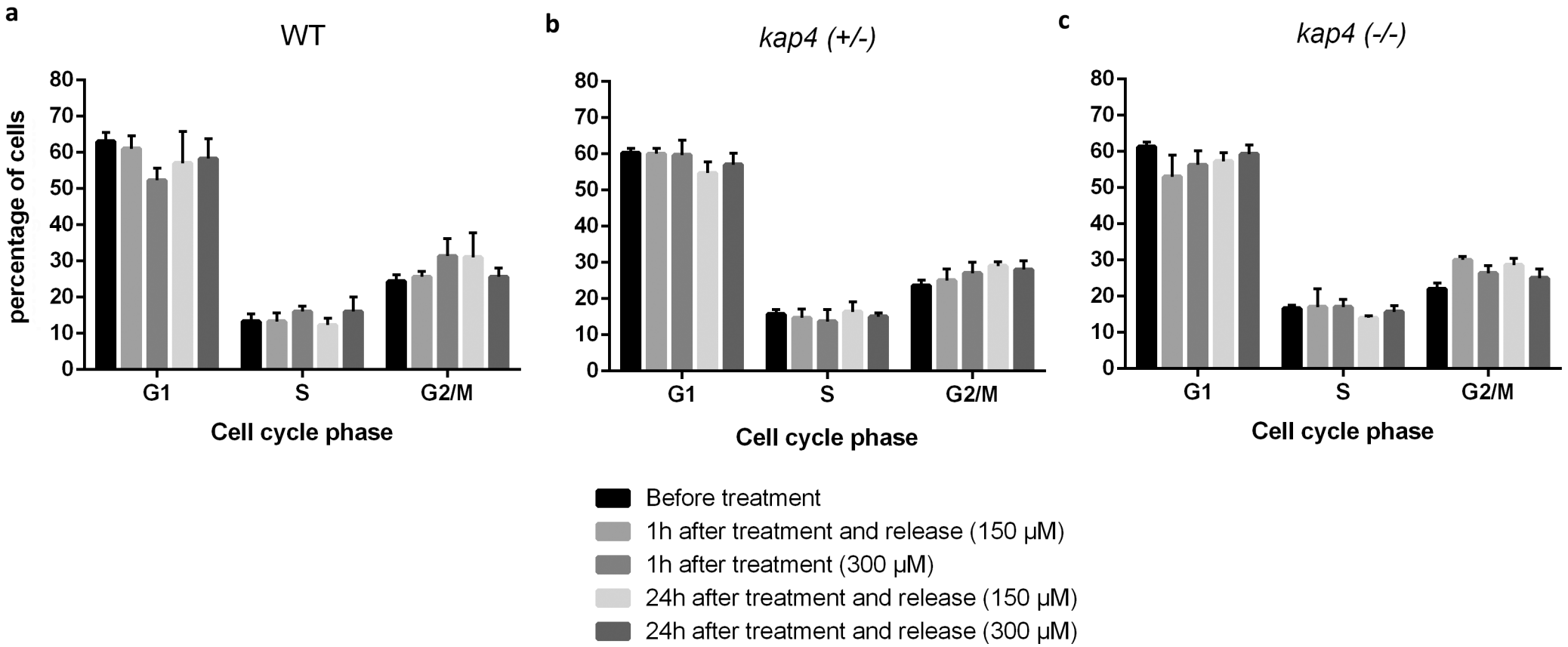

Supplementary Material 2: Flow cytometry analysis of *A. deanei* DNA content in wild type (WT) and mutant cells treated or not with cisplatin for 1 h or 24 h.

Wild type	Replicate 1		Replicate 2	
Small blank	1456	1121	1205	1190
Small NT	29656	28775	29332	29011
Small 0,25h	28744	28312	31223	30774
Small 1h	28552	28331	30999	31421
Small 3h	27561	28078	30657	30212
Small 6h	27771	26987	29044	27908
Kap4+/-	Replicate 1		Replicate 2	
Small blank	1987	1999	1024	1016
Small NT	30999	31647	32886	32543
Small 0,25h	29767	29342	31888	31369
Small 1h	30145	29987	29042	29466
Small 3h	29688	28921	33112	33876
Small 6h	27556	27899	29234	30450
Kap4-/-	Replicate 1		Replicate 2	
Small blank	1113	997	1002	996
Small NT	26684	27499	29500	29122
Small 0,25h	27312	27484	28666	27521
Small 1h	25433	26421	29311	29875
Small 3h	26911	26041	26884	28333
Small 6	25987	26020	26003	27421

Supplementary Material 3: DNA repair kinetics (0.25-6 h) measured by long-range qPCR. Absorbance values for the smaller fragments of A. deanei WT, kap4+/- and kap4-/-.